

### 5.2.3 Dimensionless parameterization

The purpose of this section is to suggest freshwater spongy spray icing parameters that may influence the dendritic ice crystal breakage/exit ratio  $A$ , to organize those parameters into dimensionless groups within an equation for  $A$ , and to discuss the meaning of the dimensionless groups as far as  $A$  is concerned.

The velocity of the airstream,  $V$ , and the diameter of the ice cylinder,  $D$ , may be the most important variables in the mechanical shearing associated with aerodynamic skin friction and heat transfer. They may in part dictate the ice crystal morphology because they influence the heat transfer responsible for crystal growth. The air velocity,  $V$ , may also control the impulse force given to the surface by the colliding droplets, and consequently dendritic breakage/dislocation and surface liquid mixing. With respect to surface collision, the flux of collected liquid mass,  $Mw$ , will be important, as the amount of water mass in collision over the cylinder surface may be significant. The present approach does not include the effect of impacting ice particles on the dendritic ice crystal breakage/exit ratio  $A$ , even though this is probably a very significant factor (Gayet, Bain and Soulage, 1984). Instead, the airborne ice crystal content is assumed to be zero in the experimental tests. Therefore, the present approach assumes only supercooled water droplets, although Gayet, Bain and Soulage (1984) demonstrate a 50% reduction of accretion mass

due to accretion surface bombardment by airborne ice crystals that result in surface breakage and exit for both wet and dry icing (a similar result is shown in Lozowski et al., 1979).

The gravitational acceleration,  $g$ , is included in the dimensional analysis, as it may influence surface liquid shedding. Gravitational acceleration in combination with centripetal acceleration and surface shearing may accentuate shedding at the bottom of the cylinder:

Macroscopic heat transfer is entrenched in the variable  $Mi_4$ , (the mass growth flux of ice) which represents the total possible accumulation of ice crystalline material.  $Mi_4$  tends to larger values for larger surface liquid undercoolings. This implies a tendency to greater dendritic morphology in the surface layer. Conversely, smaller values of  $Mi_4$  may imply smaller undercooling with a greater tendency to basal plane morphology (Hallet, 1964). Therefore,  $Mi_4$  may also influence the ice crystal breakage ratio  $A$ .

$(Mw_1 - Mi_4)$  represents the liquid mass shed flux for solid non-spongy ice growth where  $Mi_4$  is the solid accretion mass flux. If  $(Mw_1 - Mi_4)$  is small, ice crystals that have broken may not be transported away from the surface and shed. If  $(Mw_1 - Mi_4)$  is large, the surface liquid layer on a spongy accretion will tend to be either thick or flowing fast. Either result may facilitate more efficient ice particle shedding.

The cylinder rotation rate,  $\Omega$ , will influence the thermodynamics of growth through heat transfer, as described in section 4.3. In addition, the peripheral velocity of the surface will affect the relative impact velocity between the droplets and the cylinder. Hence  $\Omega$  the cylinder rotation rate in radians/second is included in the dimensionless group analysis.

Arrangement of the chosen variables ( $(Mw_1 - Mi_4)$ ,  $Mw_1$ ,  $Mi_4$ ,  $V$ ,  $\Omega$ ,  $D$ ,  $g$ ), into dimensionless groups results in a parameterization for  $A$ , the ice crystal breakage/shedding ratio. We have expressed this as:

$$A = C \left( \frac{Mw_1 - Mi_4}{Mi_4} \right)^a \left( \frac{Mw_1 - Mi_4}{Mw_1} \right)^b \left( \frac{V}{\pi D} \right)^c \left( \frac{g}{\pi^2 D} \right)^d \quad 5.6$$

Equation 5.6 may be rewritten using the freezing fraction defined as  $n_f = Mi_4 / Mw_1$ . The result is:

$$A = C \left( \frac{1}{n_f} - 1 \right)^a (1 - n_f)^b \left( \frac{V}{\pi D} \right)^c \left( \frac{g}{\pi^2 D} \right)^d \quad 5.7$$

where  $C$ ,  $a$ ,  $b$ ,  $c$  and  $d$  are arbitrary parameters which must be solved for as the basis for the empirical description of  $A$ . Equation 5.6 and 5.7 assumes a power law relationship between the dimensionless groups and  $A$ . The choice of simple

power law relationships for the dimensionless groups is an arbitrary choice not in keeping with the general nature of dimensional analysis, which allows for a more general power series dependence on the variables involved.

The first two ratios contain the freezing fraction  $n_f$  which describes in a primitive way the effect of macroscopic heat transfer on ice surface growth morphology, as suggested above, for  $Mi_4$ . Neither the third nor fourth ratios have clearly interpretable influence on the ice crystal breakage/exit ratio. Given the above parameterization for the ice crystal breakage/exit ratio, the inherent equations and assumptions of the present approach to modelling freshwater spongy spray icing follow.

### 5.3 The Equations and Assumptions

Six equations, developed in Chapters 4 and 5, can be solved for freshwater spray icing sponginess on a rotating cylinder. The six variables that must be solved for are  $Mi_2$ ,  $Mw_2$ ,  $Mi_3$ ,  $Mw_3$ ,  $Mi_4$ , and  $A$ . The relevant equations that are sufficient for determining accretion sponginess are equations 4.1, 4.2, 4.3, 4.5, 5.5, and 5.7. These are repeated here:

$$(Mi_1 + Mw_1) = (Mi_2 + Mw_2) + (Mi_3 + Mw_3) \quad 5.8$$

$$Mi_4 = f(Va, t_a, t_d, w, D, d) \quad 5.9$$

$$Mi_1 + Mi_4 = Mi_2 + Mi_3$$

5.10

$$Mi_1 + AMi_4 = Mi_3$$

5.11

$$\frac{Mi_1}{\rho_i} = \frac{Mi_2}{\rho_i} + \frac{Mw_2}{\rho_w}$$

5.12

$$A = C \left( \frac{Mw_1 - Mi_4}{Mi_4} \right)^a \left( \frac{Mw_1 - Mi_4}{Mw_1} \right)^b \left( \frac{V}{\pi D} \right)^c \left( \frac{g}{\pi^2 D} \right)^d$$

5.13

where the mass flux of collected ice particles  $Mi_1$ , the mass flux of collected water  $Mw_1$ , the wind speed  $V$ , the air temperature  $T_a$ , the droplet temperature  $t_d$ , the droplet diameter  $d$ , the cylinder diameter  $D$  and the liquid water content  $w$ , are required as input parameters in order to determine sponginess.

For the purpose of the present thesis,  $Mi_1$  is assumed to be zero for lack of better information. Since  $Mw_1$  includes the influence of the collection efficiency  $E$ , according to:

$$Mw_1 = EwD$$

5.14

the value of  $E$  must be known or estimated. For the present purpose, a parameterization of the Langmuir and Blodgett (1946) data is used on the basis of the median volume droplet diameter,  $d$ .

The present model depends on the following requirements and assumptions in modelling sponginess in freshwater spray icing on a rotating cylinder: (1) all the requisite input parameters are known, including  $Mi_1$ ,  $Va$ ,  $t_a$ ,  $t_d$ ,  $d$ ,  $D$ ,  $w$  and either  $Mw$ , or  $E$ ; (2) heat transfer from the surface on the basis of a non-rotating smooth cylinder with a surface liquid film at  $0^\circ\text{C}$ ; (3) no droplet bouncing or splashing from the surface; (4) complete liquid film mixing before shedding; (5) equitable distribution of accretion on the cylinder; (6) the radial growth velocity for the spongy ice accretion is identical to that for a solid ice accretion given the same heat transfer; (7) the volumetric flux of shed ice particles that escape in the shed liquid flow is replaced in the accreted ice by an equivalent volumetric entrapment flux of liquid in order to maintain condition 6; (8) the surface layer hypothesis is assumed to describe the accretion/shedding mechanism (as discussed in section 4.2), and (9) the empiricism inherent in equation 5.13 for determining the ice crystal breakage/exit fraction,  $A$ , is general enough to apply to all input conditions.

Conditions 6 and 7 are an interpretation of equations 5.11 and 5.12. Equation 5.11 describes the mass balance of ice particles in the surface liquid and equation 5.12 describes the volumetric accretion of the spongy growth in relation to a solid ice accretion with the same ice growth rate  $Mi_1$ .

Since the parameterizations of the ice crystal breakage/exit ratio,  $A$ , depends upon  $C$ ,  $a$ ,  $b$ ,  $c$ , and  $d$ , these must be determined on the basis of experimental data. A brief description of the experimental approach used to obtain a small data set is presented in the next section. This will be followed by a section on the data and the derivation of the empirical constants.

#### 5.4 The Experimental Method

The experiments were run to obtain freshwater ice sponginess as functions of air temperature and wind speed. The F.R.O.S.T. tunnel at the University of Alberta was used for the experimental runs. This is a closed loop refrigerated wind tunnel, capable of producing spray ice accretion under controlled conditions.

The air temperature was varied in three of the cases studied, while other important parameters (wind speed, droplet size, cylinder diameter, and liquid water content) remained constant. Changing the air temperature is an effective way to alter the thermodynamics of the spongy icing process (primarily the value of  $n_f$  in equation 5.7). Another set of data was produced by varying the wind speed while holding the other parameters constant.

The tunnel air temperature control was set at a particular value for each run, and the tunnel was allowed to come to thermal equilibrium. The F.R.O.S.T. tunnel typically experiences a cyclical temperature variation with a

peak-to-peak amplitude close to 1.0 °C at temperatures close to the freezing point. Therefore the air temperature was averaged over the accretion time.

The liquid water content at the cylinder location was measured before each run using a C.S.I.R.O. KING liquid water content probe (Knollenberg, 1981). The waterflow to the upstream spray nozzles was turned off just prior to the insertion of the rotating plexiglass cylinder into the working section of the tunnel. This was done in order to allow the cylinder temperature to reach equilibrium with the air. At temperatures close to the freezing point, this technique would allow an immediate ice formation while a cylinder initially at room temperature might not produce an accretion. The 5.0 cm plexiglass cylinder was oriented horizontally across the tunnel cross section, and was rotated at 0.5 Hz by a small direct current electric motor. Then the water was turned on, with the assumption that the liquid water content remained unchanged from the presetting. This assumption was verified many times in the course of the experimentation, as pressure and flow rate were observed to control the liquid water content well for each presetting.

The rotation rate of the cylinder was maintained at 0.5 Hz throughout the accretion interval. The cylinder and its accretion were removed from the tunnel after 10 to 15 minutes, depending on the apparent size of the formation. Since the calorimetric method used for liquid fraction measurement required a sample of ice close to 50g, a longer

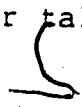


growth time was necessary at higher temperatures.

The calorimeter consisted of a vacuum flask embedded in a styrofoam shell. The lid fits into the top of the vacuum flask and a glass thermometer is inserted through the lid in such a way as to locate the mercury bulb at the centre of the vacuum flask chamber. The thermometer was accurate to  $\pm 0.05$  °C.

Initially, the flask is filled with hot tap water (45 °C to 50 °C) and the lid replaced. Before the ice sample is available, the initial hot water charge mass and temperature are recorded. Then the ice sample is carefully lowered into the hot water with the lid removed. The lid is replaced, and the operator may observe the temperature change while gently swirling the calorimeter. When the temperature stabilizes, the final temperature of the mixture is recorded along with the total mass of the calorimeter and contents. From this mass measurement, the ice sample mass can be calculated, since the calorimeter mass and hot water charge mass are known from previous measurements.

Once these temperatures and masses are known, a simple heat balance can be applied on the assumption of negligible heat loss to the container. The heat balance equation is then used to determine the sponginess of the ice sample. In this way the liquid water fraction of the sample was determined calorimetrically with an estimated absolute error of  $\pm 10$  %. This technique required careful operator attention, and had to be completed immediately after taking



the cylinder and its accreted ice out of the tunnel. Speed and care were required because the accretion would begin to drain liquid and to melt.

Since the droplet size was not measured, it was inferred from data that was collected. The method used is documented, along with the assumptions, in Appendix D.

Figures 5.1 to 5.3 show the resulting data as solid circles. Figure 5.4 shows the sensitivity of freshwater sponginess to variation in wind velocity. Examination of Figures 5.1 to 5.4 shows that the error in determining ice sponginess as functions of air temperature and velocity may be largely systematic in nature.

### 5.5 The Data and Empirical Constants

In order to use equation 5.13 in the set of equations proposed in section 5.3 to model freshwater spongy spray ice formation on a rotating cylinder, the constants  $C$ ,  $a$ ,  $b$ ,  $c$ , and  $d$  should be evaluated statistically over a large and accurate data set. However, as this is only a preliminary study of a complicated phenomenon with little available data, five points were selected from the six available data sets, and were used to solve for the five constants. This method cannot form a reliable basis for a universal model of freshwater spongy spray icing on rotating cylinders, but the performance of the model may give an indication of the potential for modelling with dimensional analysis in the future.

Four data sets produced at the University of Alberta are shown in Figures 5.1 to 5.4. Two relevant data sets from Lesin et al. (1980) are also used.

Figure 5.1 shows the experimentally determined ice fraction as a function of the air temperature and summarizes the most comprehensive data set presented. This data (represented as solid circles), was produced according to the method described in section 5.4 for a cylinder 5.0 cm in diameter, with rotational frequency 0.5 Hz, in a  $23 \text{ ms}^{-1}$  air flow with freshwater spray, having a liquid water content of  $1.7 \text{ gm}^{-3}$ . The median volume diameter was calculated to be  $16 \mu\text{m}$  according to the method described in Appendix D, and the droplet temperature was assumed to equal the air temperature. It was also assumed that there were no ice particles collected. On the basis of the data cluster, a single point (shown in Fig. 5.1 by the arrow) at an air temperature of  $-3.0 \text{ }^\circ\text{C}$  and ice fraction 84% (16% sponginess) was chosen as one of five conditions necessary for determining the set of empirical constants from equation 5.13. Also shown in Figure 5.1 are three curves that represent the performance of the model. These will be discussed in section 5.6.

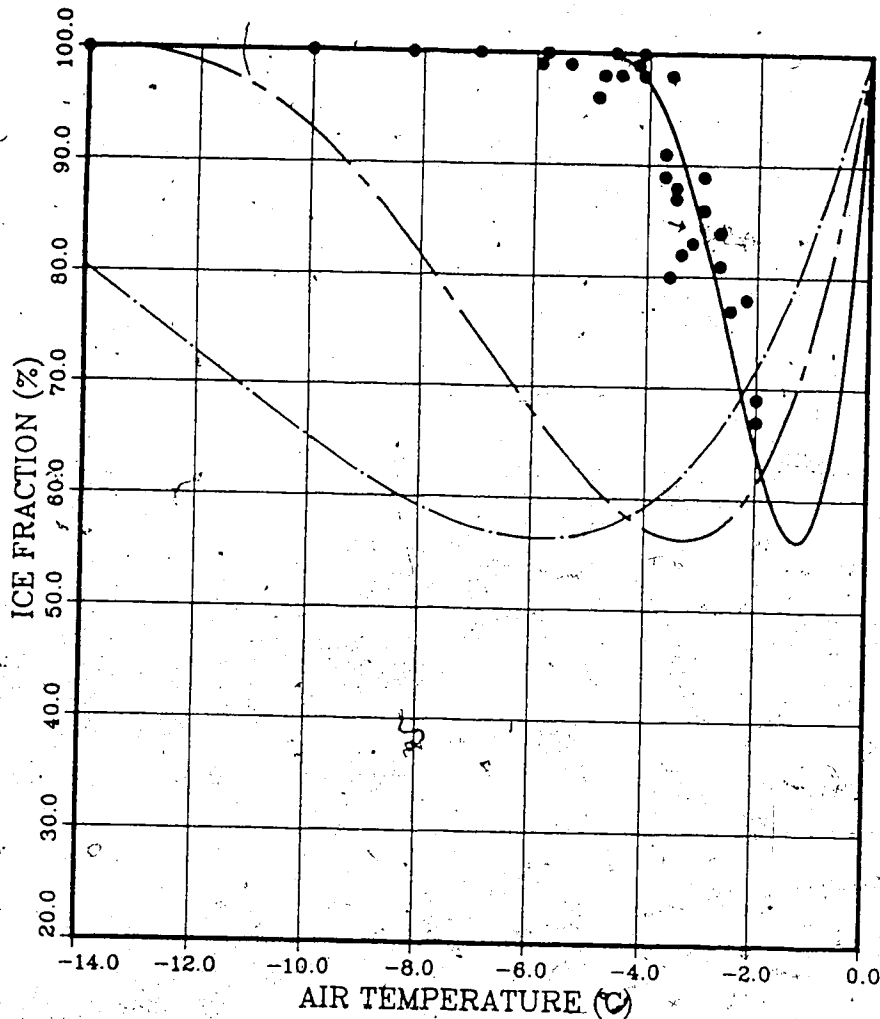


FIGURE 5.1 Ice fraction versus air temperature for spongy ice grown on a rotating cylinder over an air temperature range from 0.0 to -14.0 °C. The experimental data (shown as solid circles) was obtained with a plexiglass cylinder of a diameter  $D=5.0$  cm, a median volume drop diameter  $d=16$   $\mu\text{m}$ , an air speed  $V=23$  m/s, a liquid water content  $w=1.7$   $\text{gm}^{-3}$ , and a rotation rate  $\Omega=0.5$   $\text{s}^{-1}$ . The solid curve represents the fresh water icing model as described in section 5.3, with a liquid water content  $w=1.7$   $\text{gm}^{-3}$ . The chain-dashed curve is for the model with  $w=5.0$   $\text{gm}^{-3}$ , and the chain-dot curve, for the model with  $w=10.0$   $\text{gm}^{-3}$ . The arrow indicates the empirical anchor point taken from this data.

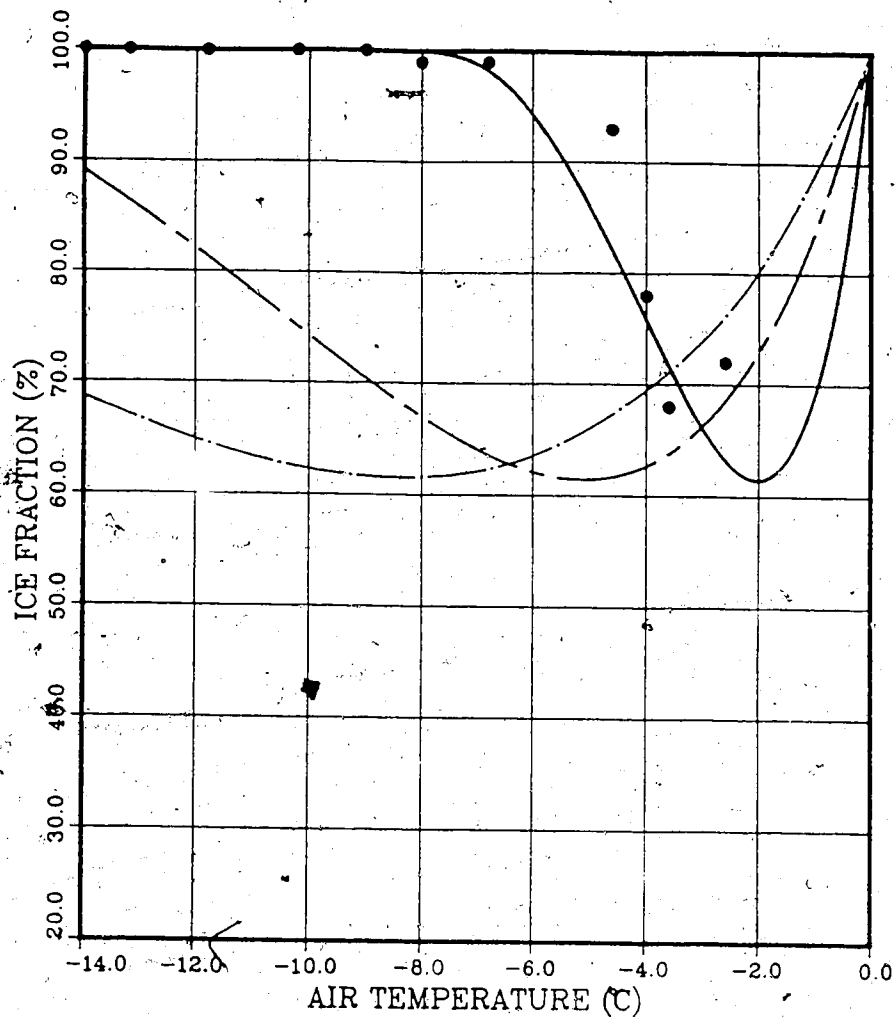


FIGURE 5.2 Ice fraction versus air temperature for spongy ice grown on a rotating cylinder over an air temperature range from 0.0 to -14.0 °C. The experimental data (shown as solid circles) was obtained with a plexiglass cylinder of diameter  $D=5.0$  cm, a median volume drop diameter  $d=20$   $\mu\text{m}$ , an air speed  $V=28$  m/s, a liquid water content  $w=1.7$   $\text{gm}^{-3}$  and a rotation rate  $\Omega=0.5$   $\text{s}^{-1}$ . The solid curve represents the freshwater icing model as described in section 5.3 with a liquid water content  $w=1.7$   $\text{gm}^{-3}$ . The chain-dashed curve is for the model with  $w=5.0$   $\text{gm}^{-3}$ , and the chain-dot curve, for the model with  $w=10.0$   $\text{gm}^{-3}$ .

The data depicted in Figures 5.2 and 5.3 are the result of the same experimental procedures as the data shown in Figure 5.1 and described in section 5.4. The experimental conditions for each data set shown in Figures 5.2 and 5.3 were used to run the model. The model performance is shown. Figure 5.2 also includes two sets of model output at different liquid water contents. No data from Figure 5.2 was used in determining the empirical constants of equation 5.13. However, one condition from Figure 5.3 (shown by the arrow) was used: the point at an ice fraction of 57.4% (sponginess 42.6%), and an air temperature of  $-2.0$ .

The data depicted in Figure 5.4, shows the dependence of ice sponginess on air velocity while the air temperature is kept at  $-5.0$  °C. Two conditions were chosen from this data (as shown by the arrows) for determination of the constants in the empirical equation 5.13: an ice fraction of 52.7 % at an air velocity of 20.0 m/s, and an ice fraction of 63.5 % at an air velocity of 30.0 m/s.

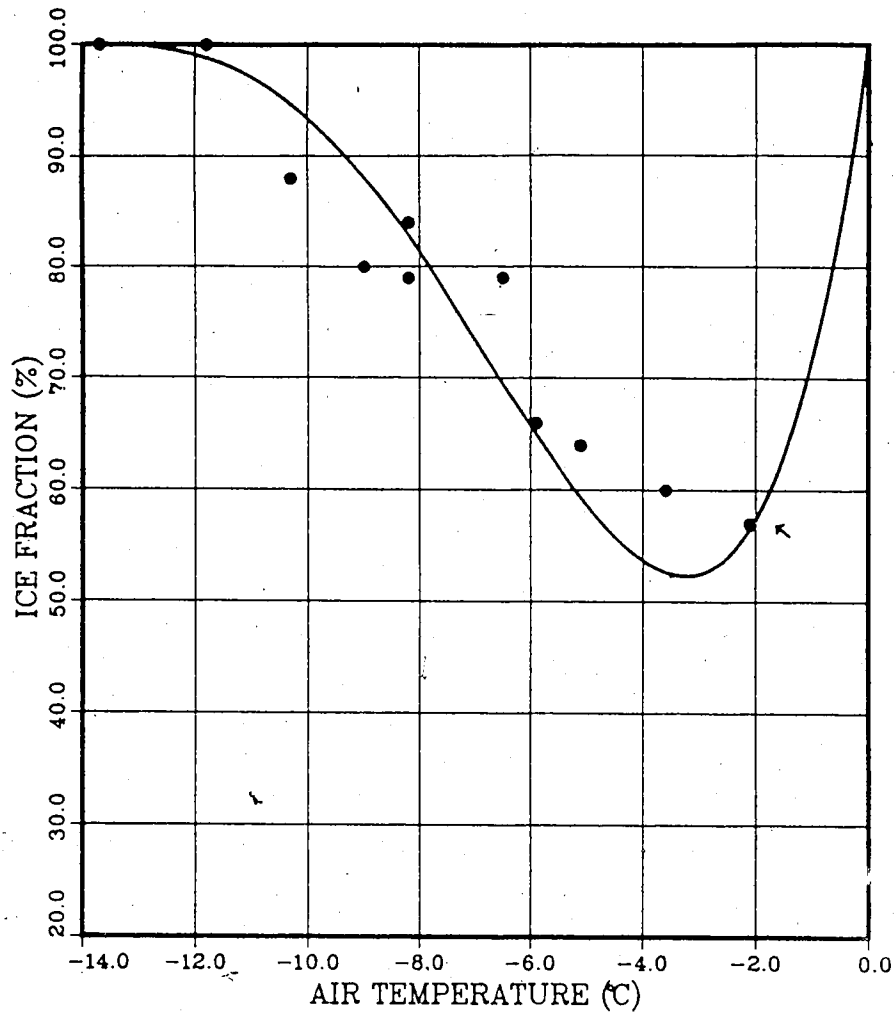


FIGURE 5.3 Ice fraction versus air temperature for spongy ice grown on a rotating cylinder over an air temperature range from 0.0 to -14.0 °C. The experimental data (shown as solid circles) was obtained with a plexiglass cylinder of diameter  $D=5.0$  cm, a median volume drop diameter  $d=25$   $\mu\text{m}$ , an air speed  $V=20$  m/s, a liquid water content  $w=3.0$   $\text{gm}^{-3}$ , and a rotation rate  $\Omega=0.5$   $\text{s}^{-1}$ . The solid curve represents the fresh water icing model as described in section 5.3 with a liquid water content  $w=3.0$   $\text{gm}^{-3}$ . The arrow indicates the empirical anchor point taken from this data.

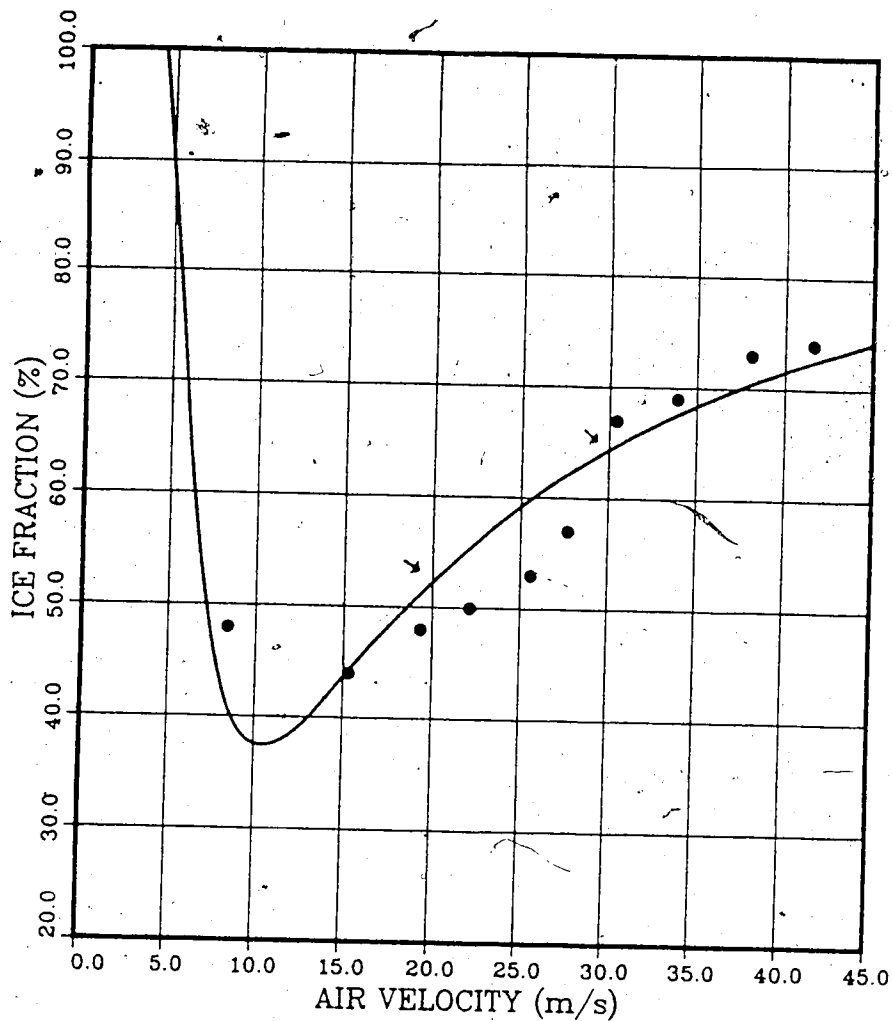


FIGURE 5.4 Ice fraction versus air speed for spongy ice grown on a rotating cylinder over an air velocity range from 0.0 to 45.0 m/s. The experimental data (shown as solid circles) was obtained with a plexiglass cylinder of diameter  $D=5.0$  cm, a median volume drop diameter  $d = 25 \mu\text{m}$ , an air temperature  $t_a = -5.0$  °C, a liquid water content  $w=4.4 \text{ gm}^{-3}$ , and a rotation rate  $\Omega=0.5 \text{ s}^{-1}$ . The solid curve represents the freshwater icing model as described in section 5.3 as a function of air speed for a liquid water content of  $4.4 \text{ gm}^{-3}$ . The arrows indicate the empirical anchor points taken from this data.



Figures 5.5 and 5.6 show data taken from the experimental work of Lesins et al. (1980). This work was performed in a closed circuit wind tunnel at the University of Toronto, with a rotating cylinder under freshwater spray icing conditions. The sponginess of freshwater accretion was measured using a centrifuge and examined as a function of liquid water content and rotation rate. The primary finding of the investigation was the dependence of sponginess on the rotation rate.

Figure 5.5 shows the experimental results of Lesins et al. (1980) for the variation of ice fraction as a function of liquid water content. The experimental conditions for the data set, are documented in the caption. The solid line represents the data which was taken over a range of air temperatures ( $-4^{\circ}\text{C} \geq t_a \geq -16^{\circ}\text{C}$ ) and is therefore an average curve produced to show the variation of ice fraction with liquid water content. This was done by Lesins et al. (1980) because ice sponginess was assumed to be essentially constant over the temperature range from  $-4$  to  $-16^{\circ}\text{C}$ . One condition used to determine the empirical constants of equation 5.13 was extracted on the basis of Figure 5.5: an ice fraction of 53% at a liquid water content of  $10 \text{ gm}^{-3}$ . For calculation purposes, the air temperature was assumed to be  $-10^{\circ}\text{C}$ . Figure 5.5 also shows the performance of the model for three different air temperatures, ( $-4^{\circ}\text{C}$ ,  $-10^{\circ}\text{C}$ ,  $-16^{\circ}\text{C}$ ), covering the specified temperature range given by Lesins et al. (1980).

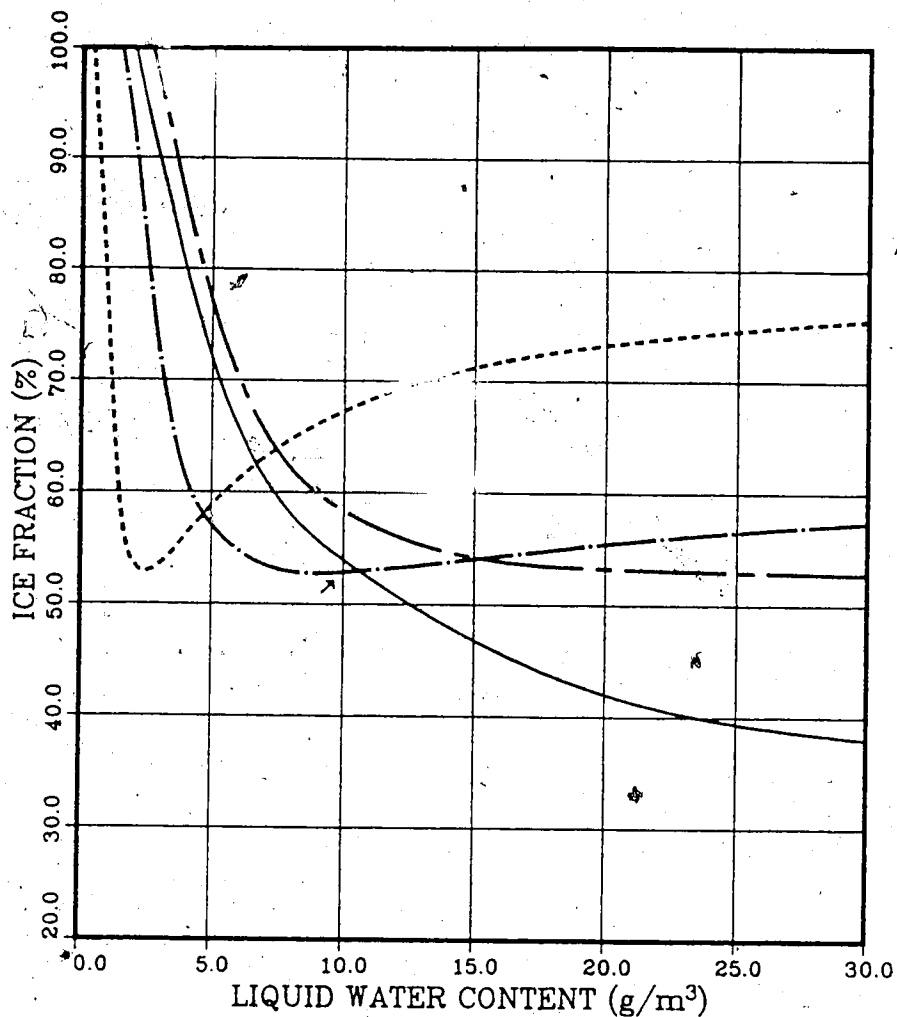


FIGURE 5.5 Ice fraction versus liquid water content for spongy ice grown on a rotating cylinder over an air temperature range from  $-4$  to  $-16$  °C. The experimental data (represented as a solid line) of Lesins et al. (1980) was obtained with a cylinder diameter  $D=1.9$  cm, a drop diameter  $d=90$   $\mu\text{m}$ , an air speed  $V=18$  m/s, and the rotation rate  $\Omega=0.5$   $\text{s}^{-1}$ . The solid curve represents the experimental data averaged for a range of air temperatures from  $-4$  to  $-16$  °C. The chain-dashed curve is the model (as described in section 5.3) output for  $-16$  °C. The chain-dot curve represents the model output for  $-10$  °C, and the dashed line shows model output for  $-4$  °C air temperature. The arrow indicates the empirical anchor point taken from this data.

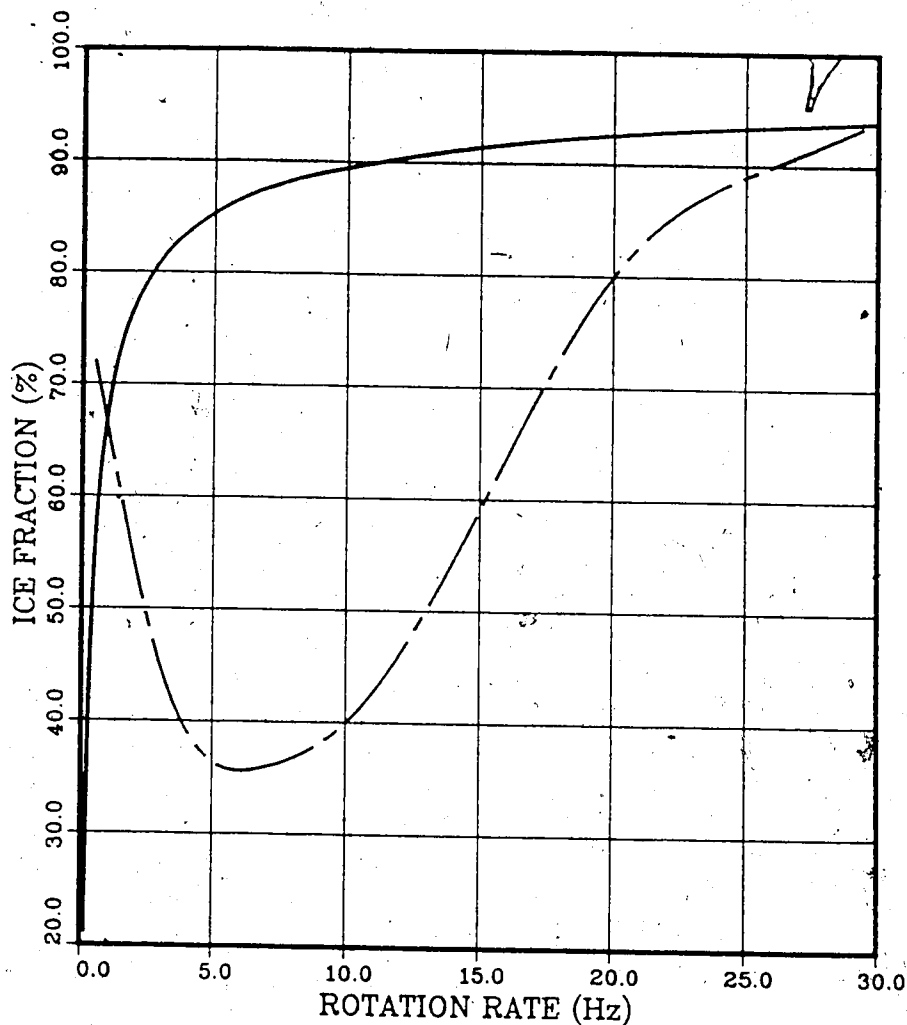


FIGURE 5.6 Ice fraction versus rotation rate for spongy ice grown on a rotating cylinder. The experimental data of Lesins et al. (1980) (shown as the chain-linked curve) was obtained with a cylinder diameter  $D=1.9$  cm, a median volume drop diameter  $d=90$   $\mu\text{m}$ , an air speed  $V=18$  m/s, a liquid water content  $w=5.0$   $\text{gm}^{-3}$ , and an air temperature  $t_a=-5.0$   $^{\circ}\text{C}$ . The solid curve shows the model (described in section 5.3) as a function of the rotation rate for the above conditions.

Figure 5.6 shows the experimental results of Lesins et al. (1980) for the variation of ice fraction as a function of rotation rate. The experimental conditions for this data set are documented in the caption. The chain-dashed line represents the data collected as a best fit curve. Figure 5.6 also shows the performance of the model under the conditions as specified by Lesins et al. (1980).

The five conditions chosen from Figures 5.1, 5.3, 5.4, and 5.5 (as indicated by the arrows) were used to solve for the five constants  $C, a, b, c, d$  found in equation 5.13. The resulting values for these empirical constants are:

$$C = 17.5$$

$$a = -0.99$$

$$b = 3.8$$

$$c = -0.66$$

$$d = 0.58$$

With the determination of these constants, the freshwater spongy icing model for rotating cylinders is capable of calculating empirically based values of sponginess. The model performance results appear along with the experimental data in Figures 5.1 to 5.6. A discussion of these results follows, in Section 5.6.

## 5.6 Model Performance

Figure 5.1 shows the model performance (as the solid curve) with the conditions responsible for the experimental data as input. The curve seems to model the data

effectively; this is to be expected, as the model is empirically dependent on a condition extracted from Figure 5.1. However, it should be kept in mind that this condition was based on only a single data point from the Figure. The main point here is not that the model is proven correct, but that the inherent empiricism appears capable of describing the available data.

Examination of Figure 5.1 also shows an interesting functional relationship between ice fraction and air temperature. As temperature changes from -5 to 0 °C, the ice fraction varies from 100% to a minimum of approximately 56% and back to 100% at the freezing temperature. In the case of freshwater accretion, the ice fraction may be expected to approach one at the dry icing condition. This will not be strictly true as even quickly freezing droplets in rime icing may exist in the liquid phase over a small time period. Therefore, the model demonstrates the reasonable expectation of predicting an ice fraction equal to one at low temperatures. The model performance has been included (in Figure 5.1) for liquid water contents of  $5.0 \text{ gm}^{-3}$  and  $10 \text{ gm}^{-3}$  in order to show that an increase in collected water will force the Ludlam limit (dry/wet icing transition point) toward lower temperature.

An interesting feature of Figure 5.1 is that the ice fraction dramatically increases to a value of one close to the freezing point. Close to the freezing point, the ice fraction (or sponginess) of an accretion may only be of

theoretical interest as: (1) low adhesion strength of ice may preclude any actual ice attachment to the rotating cylindrical surface, (2) the definition of what an ice accretion is may become uncertain when the cylinder has far more liquid water on it than ice (as the author has observed in the F.R.O.S.T. tunnel at close to freezing, many times), and (3) the mass accretion rates will be very small and for such practical purposes as ice loading design, essentially negligible. However, these points aside, it is suggested that as the air temperature approaches 0 °C, the supercooling in the surface liquid film must also approach a small value. As the supercooling becomes small, free dendritic growth is suppressed in favor of basal plane growth, which is more solid by nature than is dendritic structure. These accretions grown under air temperatures close to 0 °C will be small with respect to mass accumulation, but will be solid according to the present sponginess model. This characteristic of the model may be partially substantiated by icicle studies done by Knight (1980) and Laudise and Barns (1979). Icicles are very comparable to cylinder icing, and may be thought of as vertically oriented, non-rotating cylinders with a liquid film moving axially under air temperatures often very close to the freezing point. Laudise and Barns (1979) report that in all cases they studied, the c-axis was not oriented in the direction of the axis of the icicle, and no sponginess was found. This implies that the ice growing under the

descending liquid film was primarily growing solid in the a-axis direction (implying growth parallel to basal plane). This agrees with the present model at air temperatures close to the freezing point.

In their third concluding point, Lesins et al. (1980) briefly discuss an apparent inconsistency in their measurements of ice sponginess for a rotating cylinder in freshwater spray icing conditions. They expected great sponginess (a small ice fraction) at warm air temperatures (close to 0 °C) but instead, observed hard ice (ice fraction close to one). Examination of Figures 5.1, 5.2 and 5.3 shows that the present model of sponginess predicts ice fractions approaching one for air temperatures approaching the freezing point. Therefore, these observations of Lesins et al. (1980) also corroborate the present model, at least in this respect.

The data shown in Figure 5.2 appear to fall along the model's prediction curve (solid line). Model performance for liquid water contents of 5 gm<sup>-3</sup> and 10 gm<sup>-3</sup> have been included to once again show that the dry/wet transition is moved to lower air temperatures as the liquid water content is increased. The model predicts the same minimum ice fraction value for each of the liquid water contents shown. This is because air temperature will affect only the first two terms in equation 5.13, causing the same minimum values in  $A$  and  $\lambda_f$  to be computed.

Figure 5.3 shows a data set not independent of the present model's empiricism. One condition was derived from this figure, as stated in section 5.5. The model prediction curve (solid) as in Figure 5.1 appears to follow the data quite well with the largest datum to predicted error being 9% (absolute error). The empiricism inherent in the sponginess model appears capable of describing the available data.

Figure 5.4 shows a data set on which the spongy spray icing model is strongly dependent. Two conditions were extracted from this figure, and they are recorded in section 5.5. The model shows that as the wind speed drops, the heat transfer drops. In this case, an air velocity of 4 m/s results in solid ice growth (ice fraction of unity). As the air velocity increases above 4 m/s, dendritic surface crystal growth may be stimulated by an increased surface liquid supercooling with an increase in sponginess as a possible consequence. However, such increasing sponginess may begin to be suppressed at an air velocity of 10 m/s as a result of dendritic ice breakage and compaction by the wind. Compaction is defined here as the process by which the density of ice is increased by either rearrangement of free ice particles or by crushing of the structure. For the present, this supposition, along with those of Chapter 5 concerning dendritic breakage and shedding, will remain unsubstantiated. The model does, however, appear capable of modelling variations in sponginess for the conditions



inherent in the data set represented in Figure 5.4.

Figure 5.5 shows the results of Lesins et al. (1980) for ice fraction versus liquid water content for freshwater spongy spray icing on a rotating cylinder, as specified in the caption. Lesins averages his spongy results for air temperatures from  $-4^{\circ}\text{C}$  to  $-16^{\circ}\text{C}$  on the basis of the assumption that ice sponginess is independent of air temperature in that range of temperatures. The presently proposed model was run for air temperatures of  $-4^{\circ}\text{C}$ ,  $-10^{\circ}\text{C}$  and  $-16^{\circ}\text{C}$ , in order to facilitate comparison with the Lesins et al. (1980) averaged data. These three model curves are included in the figure and are specified in the figure caption.

The model performance shows the same general tendencies as the experimental data; however, this is to be expected as one empirical condition was extracted from Figure 5.5. The model could be considered to predict sponginess well, up to the  $10\text{ gm}^{-3}$  point, and after that the ice fraction predicted is too large, depending on which of the model curves is compared.

In a way that is similar to Figure 5.4, each of the curves in Figure 5.5 reaches 100% ice fraction. In addition, they do so before intercepting the ice fraction axis. This implies solid ice growth over a small range of liquid water contents in Figure 5.5 and from the three model curves it is apparent that the solid ice growth range increases with decreasing air temperature. This is reasonable as the rate

of heat transfer from the surface increases with lower air temperature and consequently the amount of liquid that may potentially freeze also increases. This region of Figure 5.5 for spray icing on a slowly rotating cylinder may be assumed to be similar to icicle growth.

For a given set of conditions (including air temperature) a number of icing regimes may be postulated on the basis of variation of liquid water content beginning at  $0 \text{ gm}^{-3}$ . Of course at  $0 \text{ gm}^{-3}$  there is no accretion but at the first increment of airborne liquid, the ice fraction is one, assuming an air temperature below the freezing point. The dry icing regime prevails until the Ludlam limit is reached. With a further increase in liquid water content, a surface liquid film develops in direct response. At lower liquid water contents the liquid film is thin with a small thermal mass, well mixed by droplet bombardment that eliminates large thermal gradients in the film. This condition produces a strong supercooling with dense and rapid growth. As the liquid water content is allowed to increase, the thickness and thermal mass of the film increases while the macroscopic heat flux to the airstream and ice accumulation remain unchanged. It is postulated that at some point the condition of the liquid film allows a-axis dendritic growth to become much less densely packed with resulting water inclusion. This point may be termed the sponginess limit and corresponds to the intersections of the ice fraction curves with the 100% ice fraction level in Figure 5.5. With a

further increase in liquid water content, the sponginess in the model and the spray icing data of Lesins et al. (1980) show a sharp decrease in ice fraction, possibly corresponding to a sharp increase in dendritic ice growth in the liquid film. Knight (1980) gives evidence that could be used to support this explanation, as he reports that sponginess was often found associated with surface hollows that showed characteristically thick liquid films. A glaze ice growth regime between the Ludlam limit and the sponginess limit may help explain the data in Figure 5.1. The cluster of data points between  $-6$  and  $-4$  °C gives the impression of an ice fraction that is slowly converging to one with decreasing air temperature. The apparent decrease in sponginess may not be a result of decreasing liquid inclusion but a decrease in surface liquid film mass, thus supporting the present hypothesis. Therefore, as a general tendency, sponginess may increase in response to thick liquid films that may result from higher liquid water contents in freshwater spray icing conditions as shown in Figure 5.5.

Figure 5.6 shows the results of Lesins et al. (1980) for the dependence of ice fraction on rotation rate of a cylinder undergoing freshwater spray accretion. Figure 5.6 demonstrates no agreement whatever (except at high rotation rates) between the Lesins et al. (1980) experimental data, and the present model of freshwater spongy spray ice formation. The Lesins et al. (1980) data show a sharp

decrease in ice fraction with increase in rotation rate at low rotation rates ( $0 < \Omega < 5$  Hz), and an apparently asymptotic approach to an ice fraction of unity at high rotation rates. The present model simply starts at the origin and asymptotically approaches an ice fraction of one. The fact that the model will predict no ice formation at  $\Omega=0$ , implies that the present model is incapable of reliably modelling the influence of rotation on sponginess. This feature of the model performance is the result of assuming that the dimensionless groups are related to the crystal breakage/exit ratio,  $A$ , by power law relationships. Therefore, it is to be expected that as  $\Omega \rightarrow 0$ ,  $\Omega$ , taken to a particular power, will either be undefined or 0. In this case, as  $\Omega \rightarrow 0$ ,  $A \rightarrow \infty$  and because all of the ice is assumed to be shed,  $\lambda \rightarrow 1$ , which implies that there is no ice accretion at all. On the other hand, the approach of ice fraction to one as a result of increased rotation rates may be expected as water is forced from the ice accretion by centrifugal force. In fact, rotation has been used to determine sponginess by measuring weight before and after centrifuging.

The reason for the large discrepancy between the curves in Figure 5.6 is probably due to the arbitrary choice of power law relationships in the dimensional analysis. However, it may also have to do with the formation of the surface lobes and knobs as observed by Lesins. The growth of surface roughness would alter the heat transfer

significantly from the smooth cylinder assumed in the model. It would give the surface liquid film protection from wind shear, producing thicker liquid films behind and around knobs and ridges, than on the exposed tops. These variations in heat transfer and liquid film thicknesses are not taken into account in the model. Therefore, it may be difficult to amend the model in such a way as to improve the prediction of sponginess as a function of rotation rate, until these complexities can be taken into account with a more general form of dimensional analysis.

## 6. CONCLUSIONS AND RECOMMENDATIONS

The ability to model sponginess in spray icing may help in responding to some types of icing problems, and the fundamentals of solidification are valuable in understanding sponginess, especially the growth of dendritic structures capable of containing water.

The Makkonen (1987) sea spray icing model and the University of Alberta ship icing model apply conservation of heat energy and mass to the spongy spray ice growth process. These two principles were also applied in this thesis to produce a new model which includes a set of hypotheses concerning the spongy growth process at the accretion surface. An empirical description of this mechanism is proposed, and examined in the light of six data sets.

In freshwater spongy spray icing the heat transfer direction may result in unconstrained solidification. Where supercooling is sufficient, the resulting growth may be dendritic with subsequent entrapment of water in the structure. In contrast, growth of sea ice demonstrates the fundamentally different process of constrained solidification in which solute build-up at the interface may be mostly responsible for a growing structure that entraps brine. The growth of sea ice typically appears as a platelet structure, whereas freshwater spongy spray ice may show a fine dendritic substructure.

Makkonen (1987) starts the development of a spongy spray icing model for a cylinder by assuming a salt balance

for collected, accreted and shed brine. As a result, the effective distribution coefficient ( $k=S_i/S_w$ ) is found to be a function of the interfacial distribution coefficient ( $k^*=S_i/S_b$ ) and  $n$ , the accretion fraction of a spongy saline spray ice accretion.  $k^*$  is shown to be equivalent to sponginess in sea spray icing, and a first working hypothesis is presented that assumes  $k^*=0.26$ . This hypothesis is based on the results from a number of sea ice growth investigations and an analogy between salt entrapment in sea ice growth and sponginess in spray icing. The cylinder icing model of Makkonen (1984) is used to evaluate the accretion fraction,  $n$ , and the resulting model predicts accretion rates and sponginess with an iterative procedure. The details of this approach are examined in section 3.1.

Makkonen (1987) has given an interpretation for  $k^*$  which implies that the surface liquid salinity in sea spray spongy ice accretion is the same as the salinity of the entrapped brine. One physical interpretation of this result is that surface liquid may flow more or less freely through the internal ice structure; this has been termed filtration accretion/shedding. Another interpretation of  $k^*$  is advanced which depends upon the possibility of the surface liquid having a different salinity than the permanently entrapped brine. A characteristic implied by this interpretation is that the growing surface layer is distinct from and sealed off from the deeper substructure. This has been termed

surface accretion/shedding. If surface accretion/shedding is assumed, then two ice mass balances are possible--one for the liquid film and one for the whole surface accretion/shedding layer. Adoption of these two mass balances result in two equations that along with the overall mass and heat balance, result in a partial framework for a freshwater spongy spray icing model.

A surface growth assumption is made in such a way that the radial growth velocity of an assumed solid ice accretion equals the velocity of the progress of the spongy icing surface. (This assumption is part of the model's empiricism; it must be emphasized that the model predicts sponginess of accretions only, and not mass accretion rates.) In addition, it is assumed that the rate of volumetric inclusion of liquid into the structure of the spongy ice equals the shed ice particle volumetric flux. Thus the volumetric flux of ice particles controls the sponginess,  $\lambda_f$ , and is modelled empirically.

The empiricism chosen shows the feature that as the solid ice freezing fraction  $n_f \rightarrow 1$  or  $n_f \rightarrow 0$  the ice crystal breakage/exit ratio  $A \rightarrow 0$ . Thus a freshwater spongy spray icing model has been described for rotating cylinders that was tuned to five conditions from four data sets. The model in this way has shown that it is capable of describing accretion sponginess on rotating cylinders under variations of air temperature, air velocity and liquid water content. The model was found to be very poor in describing variations



in sponginess with the rate of cylinder rotation, probably due to the assumption that  $\Omega$  is related to sponginess through a simple power law relationship.

Because power law relationships are monotonic, a more complex form of relationship may be needed to model the variation of sponginess with rotation rate. The present study represents preliminary work and future approaches will likely benefit from a more rigorous use of dimensional analysis.

The understanding of surface growth processes is essential to modelling sponginess. The present thesis presents a model in which hypothetical surface processes were modelled empirically. The development of a better knowledge of these and other processes may depend largely on effective experimental work in the future.

Recommendations for future investigations include:

(1) To develop techniques to better measure the parameters in spongy spray ice growth. For instance, speedy and efficient measurement of sponginess and mass loads are needed. The drainage of liquid from a sample that is being weighed for total mass will distort a subsequent sponginess test on that sample. Possibly the best would be a technique that would accomplish both measurements at once, for example a calorimetric procedure which measures the sample mass produced by an effective and reliable sampling technique. Another possibility would be to use photographic or video records of the accretion dimensions and once the average

accretion sponginess is known, a total accretion mass may be calculated.

Since the shed flux may relate directly to processes on or in the accretion that could influence sponginess, the shed flux should be examined. While the amount of water substance shed as well as the relative amounts of ice and liquid are important characteristics to measure, the obstacles to such measurements appear considerable. For example, identifying droplets that have formed as a result of shedding may be difficult because they may be indistinguishable from droplets in the carrier air stream. Furthermore, once identified, it may be difficult to capture only the shed droplets, a process further complicated by the need to measure the fraction of ice in the shed droplets. Determining the ice fraction of the shed flux may require a technique that does not promote either droplet heat loss or nucleation that could alter the ice fraction artificially. However, one approach to the measurement of the shedding flux might be to design a technique that gives a reliable determination of the collected flux, which, with an accurate measurement of the accretion rate, could be used to determine the shedding flux.

(2) To investigate the ice fraction of accretions grown in spray conditions near the freezing point. This may help to substantiate the hypothesis presented here, that the ice fraction of spongy spray ice accretion tends towards unity

as the air temperature approaches the freezing point.

(3) To investigate the sponginess structure of accretions in order to determine if shedding is primarily a surface phenomenon or whether liquid may flow through the ice substructure before shedding. An investigation like this might reveal two distinctly different shedding mechanisms, as postulated in this thesis, which might be responsible for distinct and identifiable icing regimes for spongy spray icing.

(4) To investigate the crystallographic orientations of ice crystals in spongy spray ice accretions in order to relate surface ice crystal growth to the sponginess of the accretion. The accretion substructure may show evidence that ice dendrites have grown and broken off, with subsequent distribution and compaction onto the accretion surface. In contrast, it may be found that ice dendrites grow without breakage and that the nature of their growth determines the nature of the resulting sponginess. A greater knowledge of the micro-processes of growth on the surfaces of spongy spray ice formations will be of importance if better physical models of sponginess are to be developed.

## Bibliography

- Aksjutin, I.L., 1979: Icing of ships (in Russian). Sudostroyenye Publishing House, Leningrad, 126 pp.
- Bain, M. and Gayet, J.F., 1983: Contribution to the modelling of the ice accretion process: ice density variation with the impacted surface angle. Proceedings, First International Workshop on Atmospheric Icing of Structures, U.S. Army Cold Regions Research and Engineering Laboratory Special Report 83-17, 13-20.
- Burton, J.A., Prim, R.C. and Slichter, W.P., 1953a: The distribution of solute in crystals grown from melt. Part I: Theoretical. J. Chem. Phys., 21, 1987-1991.
- Burton, J.A., Kolb, E.D., Slichter, W.P., and Struthers, J.D., 1953b: Distribution of solute in crystals grown from the melt. Part II: Experimental. J. Chem. Phys., 21, 1991-1995.
- Cansdale, J.T., and McNaughton, I.I., 1977: Calculation of surface temperature and ice accretion rate in a mixed water droplet/ice crystal cloud. Tech. Rep. 77090, Royal Aircraft Establishment, Farnborough, U.K., 29pp.
- Chalmers, B., 1964: Principles of solidification. John Wiley and Sons, New York, 319pp.
- Cox, G.F.N. and Weeks, W.F., 1975: Brine drainage and initial salt entrapment in sodium chloride ice. U.S.A. Cold Regions Research and Engineering Laboratory, Research Report 354, 85pp.
- Druez, J., Laforte, J.L., and Nguyen, D.D., 1984: Mechanical properties of atmospheric ice. Proceedings, 2nd International Workshop on Atmospheric Icing of Structures, Trondheim, Norway, June 19-21, 1984, 51-56.
- Gayet, J.F., Bain, M., and Soulage, R.G., 1984: Role of ice crystals on ice accretion processes. Proceedings, 2nd International Workshop on Atmospheric Icing of Structures, Trondheim, Norway, June 19-21, 1984, 65-69.
- Garabedian, H., and Strickland-Constable, R.F., 1974: Collision breeding of ice crystals. Journal of Crystal Growth, 22, 188-192.
- Hallett, J., 1964: Experimental studies of the crystallization of supercooled water. Journal of the Atmospheric Sciences, 21, 671-682.

- Harrison, J.D., and Tiller, W.A., 1963: Controlled freezing of water. In Ice and snow: processes, properties and applications (ed. by W.D. Kingery). M.I.T. Press, Cambridge, 215-225.
- Hillig, W.B., 1958: Kinetics of freezing in ice in the direction perpendicular to the basal plane. In, Growth and perfection of crystals: Cooperstown Conference Proceedings, Wiley, New York, 350-359.
- Hillig, W.B. and Turnbull, D., 1956: Theory of crystal growth in undercooled pure liquids. *Journal of Chemical Physics*, 24, 914.
- Hobbs, P., 1974: Ice Physics. Oxford University Press, 837pp.
- Kachurin, L.G., 1962: The theory of aircraft icing. (in Russian) *Bull. (Izv.) Acad. Sci. USSR, Geophys. Ser.*, 6, 823-832.
- Knight, C.A., 1980: Icicles as crystallization phenomena. *Journal of Crystal Growth*, 49, 193-198.
- Knight, C.A., 1968: On the mechanisms of spongy hailstone growth. *J. Atmos. Sci.*, 25, 440-457.
- Knollenberg R.G., 1981: Techniques for probing cloud microstructure, In, *Clouds: their formation, optical properties and effects* (ed. by P.V. Hobbs and A. Deepak). Academic Press, New York, 15-91.
- Kochtubajda, B. and Lozowski, E.P., 1985: The sublimation of dry pellets used for cloud seeding. *Journal of Climate and Applied Meteorology*, 24:6, 597-605.
- Kreith, F., 1969: Principles of heat transfer. International Textbook Co., Scranton, Penn., 620pp.
- Kurz, W., and Fisher, D.J., 1986: Fundamentals of Solidification. Trans Tech Publications, Switzerland, 241pp.
- Langer, J.S. and Muller-Krumbhaar, H., 1977: Stability effects in dendritic crystal growth. *Journal of Crystal Growth*, 42, 11-14.
- Langmuir, I. and Blodgett, K.M., 1946: A mathematical investigation of water droplet trajectories. In: *Collected Works of I. Langmuir*. Pergamon Press, 10, 348-393.
- Laudise, R.A., and Barns, R.L., 1979: Are icicles single crystals? *Journal of Crystal Growth*, 46, 379-386.

- Lesins, G.B., List, R. and Joe, P.I., 1980: Ice Accretions, Part I: Testing of new atmospheric icing concepts. *J. Rech. Atmos.*, 14, 347-356.
- List, R., 1963: General heat and mass exchange of spherical hailstones. *Journal of the Atmospheric Sciences*, 20, 189-197.
- List, R., 1977: Ice accretions on structures. *J. Glaciol.*, 81, 451-465.
- Lozowski, E.P. and Gates, E.M., 1987: On the modelling of ice accretion. Invited paper in "Freezing and Melting Heat Transfer in Engineering", K.C. Cheng, editor, 84pp, (in press).
- Lozowski, E.P., Stallabrass, J.R., and Hearty, P.F., 1979: The icing of an unheated non-rotating cylinder in liquid water droplet -- ice crystal clouds. National Research Council Canada Report LTR-LT-96.
- Ludlam, F.H., 1950: The composition of coagulation elements in cumulonimbus. *Quarterly J. R. Met. Soc.*, 76, 52-58.
- Ludlam, F.H., 1951: The heat economy of a rimed cylinder. *Quarterly J. R. Met. Soc.*, 77, 663-666.
- Makkonen, L., 1985: Heat transfer and icing of a rough cylinder. *Cold Regions Science and Technology*, 10, 105-116.
- Makkonen, L., 1984: Modelling ice accretion on wires. *Journal of Climate and Applied Meteorology*, 23, 929-939.
- Makkonen, L., 1987: Salinity and growth rate of ice formed by sea spray. *Cold Regions Science and Technology*, 14, 162-171.
- Panov, V.V., 1976: Icing of ships (in Russian). *Arkticheskii i Antarkticheskii Nauchno-Issledovatel'skii Institut*, Leningrad, Trudy No. 336, 263pp.
- Plazinic, S. and Miljkovic, N., 1982: Damages of structures due to ice and wind. *Proceedings of First International Workshop Atmospheric Icing of Structures*. Hanover, New Hampshire, USA, June 1-3, 1982, 225-237.
- Savyel'ev, B.A., 1971: Structure, chemical content and strength of the accretions formed on materials (in Russian). "Zhizn'ziemli" ("Life of the Earth"), No. 7, 23-33.

Terwillegar, J.P. and Dizio, S.F., 1970: Salt rejection phenomena in the freezing of saline solutions. Chem. Eng. Sci., 25, 1331-1349.

Weeks, W.F. and Ackley, S.F., 1982: The growth structure and properties of sea ice. U.S.A. Cold Regions Research and Engineering Laboratory, CRREL Monograph 82-1.

Weeks, W.F. and Lofgren, G., 1967: The effective solute distribution coefficient during the freezing of NaCl solutions. In, Physics of Snow and Ice (ed by H. Oura), Institute of Low Temperature Science, Hokkaido Vol. I, No. 1, 579-597.

Weeks, W.F. and Gow, A.J., 1978: Preferred crystal orientations along the margins of the Arctic Ocean. J. Geophys. Res., 84, no. C10, 5105-5121.

Zakrzewski, W.P., Blackmore, R.Z., and Lozowski, E.P., 1987: Mapping the ice growth rates on sea-going ships in waters east of Canada. In, Proceedings of 2nd Canadian Workshop on Operational Meteorology, Halifax, N.S., October 14-16, 1987, 77-99.

Zakrzewski, W.P., Blackmore, R.Z., Lozowski, E.P., and Muggerridge, D., 1987: An improved ship spraying model. Unpublished manuscript, The University of Alberta, Division of Meteorology. Also, Journal of Geophysical Research (in preparation).

Zakrzewski, W.P. and Lozowski, E.P., 1987: The application of a vessel spraying model for predicting ice growth rates and ice loads on a ship. In, Proceedings of the 9th International Conference on Port and Ocean Engineering under Arctic Conditions, Fairbanks, Alaska, August 16-22, 1987 (in press).

Zukauskas, A., 1972: Heat transfer from tubes in cross flow. Advances in Heat Transfer, 8, 93-160.

## Appendix A

### An Examination of the Algebraic Meaning of the Interfacial Solute Distribution Coefficient $k^*$

The following derivation will show that the interfacial distribution coefficient  $k^*$  may be a function of  $\lambda_s$  the sponginess and  $J_0$  the ice fraction of the shed flux.

First define the overall salinity for the accretion  $Si_2$  and the overall salinity for the shed flux  $Si_3$ , as:

$$Si_2 = \frac{Ms_2}{Mi_2 + Ms_2 + Mw_2} \quad A.1$$

$$Si_3 = \frac{Ms_3}{Mi_3 + Ms_3 + Mw_3} \quad A.2$$

where the mass flux variables (in units of  $kgm^{-1}s^{-1}$ ) are:

$Mi_2$  - the mass flux of ice accreted.

$Ms_2$  - the mass flux of salt accreted.

$Mw_2$  - the mass flux of pure water accreted.

$Mi_3$  - the mass flux of shed ice.

$Ms_3$  - the mass flux of shed salt mass.

$Mw_3$  - the mass flux of shed pure water.

The salinity of entrapped brine in the accretion  $Sb_2$  and the salinity of the shed brine  $Sb_3$  are defined as:

$$Sb_2 = \frac{Ms_2}{Ms_2 + Mw_2} \quad A.3$$

$$Sb_3 = \frac{Ms_3}{Ms_3 + Mw_3} \quad A.4$$



The interfacial solute distribution coefficient  $k^*$  may be defined as:

$$k^* = \frac{Si_2}{Si_3} \quad \text{A.5}$$

Introducing  $Sb_2$  into equation A.5 gives:

$$k^* = \left(\frac{Si_2}{Sb_2}\right) \left(\frac{Sb_2}{Si_3}\right) \quad \text{A.6}$$

The ratio  $(Si_2/Sb_2)$  in equation A.6 is a parameter that we can term the saline sponginess of the accretion  $\lambda_s$ ; it can be shown that:

$$\lambda_s = \frac{Ms_2 + Mw_2}{Mi_2 + Ms_2 + Mw_2} \quad \text{A.7}$$

Equation A.6 can therefore be rewritten as:

$$k^* = \lambda_s \left(\frac{Sb_2}{Si_3}\right) \quad \text{A.8}$$

Equation A.8 shows the general nature of the present derivation since  $Sb_2$  does not necessarily equal  $Si_3$ .  $Sb_2$ , the salinity of the entrapped brine, may be different from the equilibrium salinity of the surface liquid  $Si_3$ , which is assumed to be the same as the salinity of the shed brine. Algebraic rearrangement of the ratio  $(Sb_2/Si_3)$  may be written:

$$\left(\frac{Sb_2}{Si_3}\right) = \left(\frac{Ms_2}{Ms_3}\right) \left(\frac{Mi_3 + Ms_3 + Mw_3}{Ms_2 + Mw_2}\right) \quad \text{A.9}$$

The ratio of  $Ms_2$  and  $Ms_3$  describes the division of salt mass between shedding and deposition by the icing process.

We have called this  $\eta$ , the salt mass distribution

coefficient.

$$\eta = \left( \frac{Ms_2}{Ms_3} \right) \quad \text{A.10}$$

The right hand factor in Equation A.9 can be rearranged in terms of  $J_1$  and  $J_0$ .  $J_1$  is called the liquid incorporation ratio. It describes the degree to which the available surface brine on a spongy deposit is incorporated into the growing structure.  $J_0$  is the shed ice fraction. It is the mass fraction of ice in the shed flux.  $J_1$  and  $J_0$  are given by:

$$J_1 = \frac{Ms_2 + Mw_2}{Ms_2 + Mw_2 + Ms_3 + Mw_3} \quad \text{A.11}$$

$$J_0 = \frac{Mi_3}{Mi_3 + Ms_3 + Mw_3} \quad \text{A.12}$$

Algebraic manipulation of equation A.9 with the parameters defined in A.10, A.11 and A.12, results in:

$$\left( \frac{Sb_2}{Si_3} \right) = \eta \left( \frac{1 - J_1}{J_1} \right) \left( \frac{1}{1 - J_0} \right) \quad \text{A.13}$$

The substitution of equation A.13 into equation A.8 results in:

$$k^* = \lambda_s \eta \left( \frac{1 - J_1}{J_1} \right) \left( \frac{1}{1 - J_0} \right) \quad \text{A.14}$$

Thus, the interfacial distribution coefficient is dependent upon the accretion sponginess as well as three other process-describing parameters.  $k^*$  is dependent on the sponginess of the accretion  $\lambda_s$  and this Makkonen (1987) has also suggested. However,  $k^*$  also depends upon  $\eta$  a parameter that by its definition describes the distribution of salt

for the spongy spray icing process.  $\eta$  is probably related to the degree of solute build-up at the growing interface and the effectiveness with which the solute is transported away from the interface or into the accretion.  $k^*$  is also related to  $J_1$ , which is a parameter that reflects the tendency for liquid to stay in the accretion and not exit from the surface.  $k^*$  is also a function of  $J_0$ , which is defined as the ice mass fraction of the shed flux. One source of shed ice particles that might be associated with conditions at the interface of the accretion is dendritic ice crystal breakage. Therefore, equation A.14 shows that  $k^*$  depends upon the salt, pure water and ice crystal distribution mechanisms at work on the surface of sea spray spongy ice formation.

However, it is of interest to examine the influence of complete film mixing on equation A.14. Complete mixing in the liquid film may mean that the salinity of the shed water equals the salinity of the initially incorporated brine (ie. no solute build-up at the interface). This is can be represented as:

$$Sb_3 = Sb_2 \quad \text{A.15}$$

Rearrangement of equation A.15 with the parameters as defined in equations A.10 and A.11 yields:

$$\eta = \frac{J_1}{(1 - J_1)} \quad \text{A.16}$$

Substitution of equation A.16 into A.14 results in a simplification of the  $k^*$  equation. In this case  $k^*$  depends only on the sponginess  $\lambda_s$ , and the shed ice fraction  $J_0$ , under the assumption of complete mixing.

$$k^* = \frac{\lambda_s}{(1 - J_0)}$$

A.17

## Appendix B

### Derivation of the Ice Growth Flux Equation

The mass of ice grown at the surface of the cylinder may be modelled by assuming a heat balance. The heat balance is:

$$Q_1 = Q_2 + Q_3 + Q_4 + Q_5 \quad \text{B.1}$$

$Q_1$  is the latent heat of fusion which is released as pure ice crystals grow.  $Q_2$  is the heat lost from the surface of the cylinder through convective heat transfer.  $Q_3$  is the evaporative heat transfer component.  $Q_4$  is the sensible heat flux associated with bringing the impinging mass of ice and water to the equilibrium temperature of the icing surface.  $Q_5$  is the radiative heat flux component directed from the icing surface to the surrounding environment. All the heat components ( $Q_1$  to  $Q_5$ ) are in units of  $\text{Jm}^{-2}\text{s}^{-1}$ .

Given  $Q_1$ , the mass growth rate is determined according to:

$$Q_1 = \dot{M}_i L_f \quad \text{B.2}$$

where  $\dot{M}_i$  is the mass of ice grown per second per meter of cylinder length and  $L_f$  is the latent heat of fusion for pure ice at  $0.5^\circ\text{C}$ .

$Q_2$  is defined as:

$$Q_2 = \pi D h (t_s - t_a)$$

B.3

where  $D$  is the diameter of the cylinder,  $h$  is the overall heat transfer coefficient,  $t_s$  is the surface temperature of the cylinder and  $t_a$  the air temperature.

$Q_3$  is defined as:

$$Q_3 = \pi D h \left( \frac{Pr}{Sc} \right)^{0.63} \left( \frac{\epsilon L_e}{c_p P_a} \right) (e_s - e_a)$$

B.4

where  $Pr$  is the Prandtl number,  $Sc$  is the Schmidt number,  $\epsilon$  is 0.622,  $L_e$  is the latent heat of vaporization,  $c_p$  is the specific heat of air at constant pressure,  $P_a$  is the air pressure,  $e_s$  is the saturation vapor pressure at the icing surface and  $e_a$  is the actual vapor pressure in the air.

$Q_4$  is defined as:

$$Q_4 = (M_i C_i + M_w C_w) (t_s - t_d)$$

B.5

where  $M_i$  is the impinging mass flux of ice particles,  $C_i$  is the specific heat of ice,  $M_w$  is the impinging mass of water,  $C_w$  is the specific heat of water,  $t_s$  is the surface temperature (assumed equal to 0 °C) and  $t_d$  is the droplet temperature.

$Q_5$  is defined as:

$$Q_5 = \pi D \sigma a (t_s - t_a)$$

B.6

where  $\sigma$  is the Stefan-Boltzmann constant and 'a' is a linearizing factor,  $t_s$  is the surface temperature, and  $t_a$ ,

the air temperature, is taken to be the temperature of the surroundings.

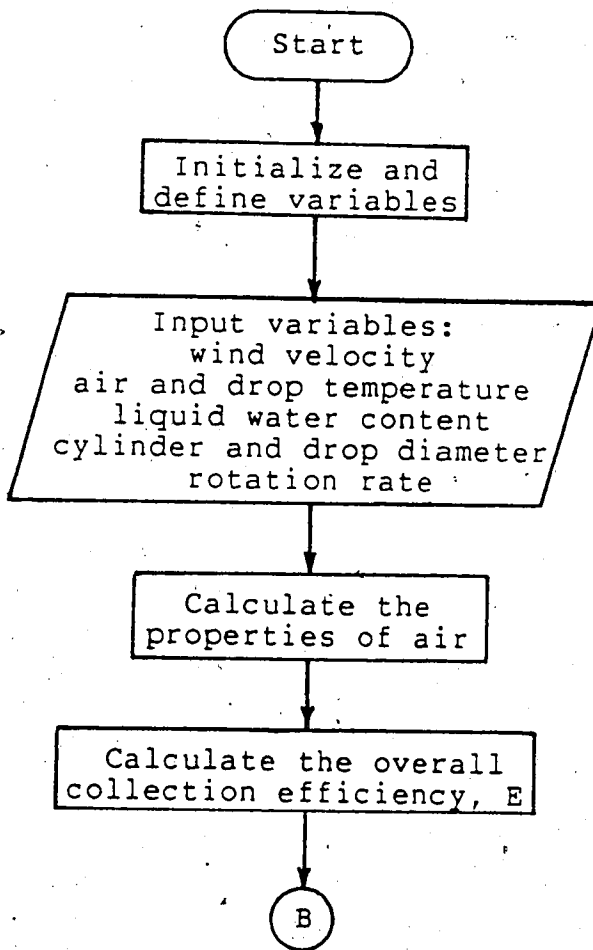
Equations B.2 through B.6 may be substituted into equation B.1 and solved for  $Mi_a$  to yield equation:

$$Mi_a = \frac{\pi Dh}{L} \left[ (t_s - t_a) + \left( \frac{Pr}{Sc} \right)^{0.63} \left( \frac{\epsilon L}{c_p Pa} \right) (e_s - e_a) \right] + L^{-1} [(Mi_i c_i + Mw_i c_w)(t_s - t_a)] + L^{-1} \pi D \alpha (t_s - t_a) \quad B.7$$

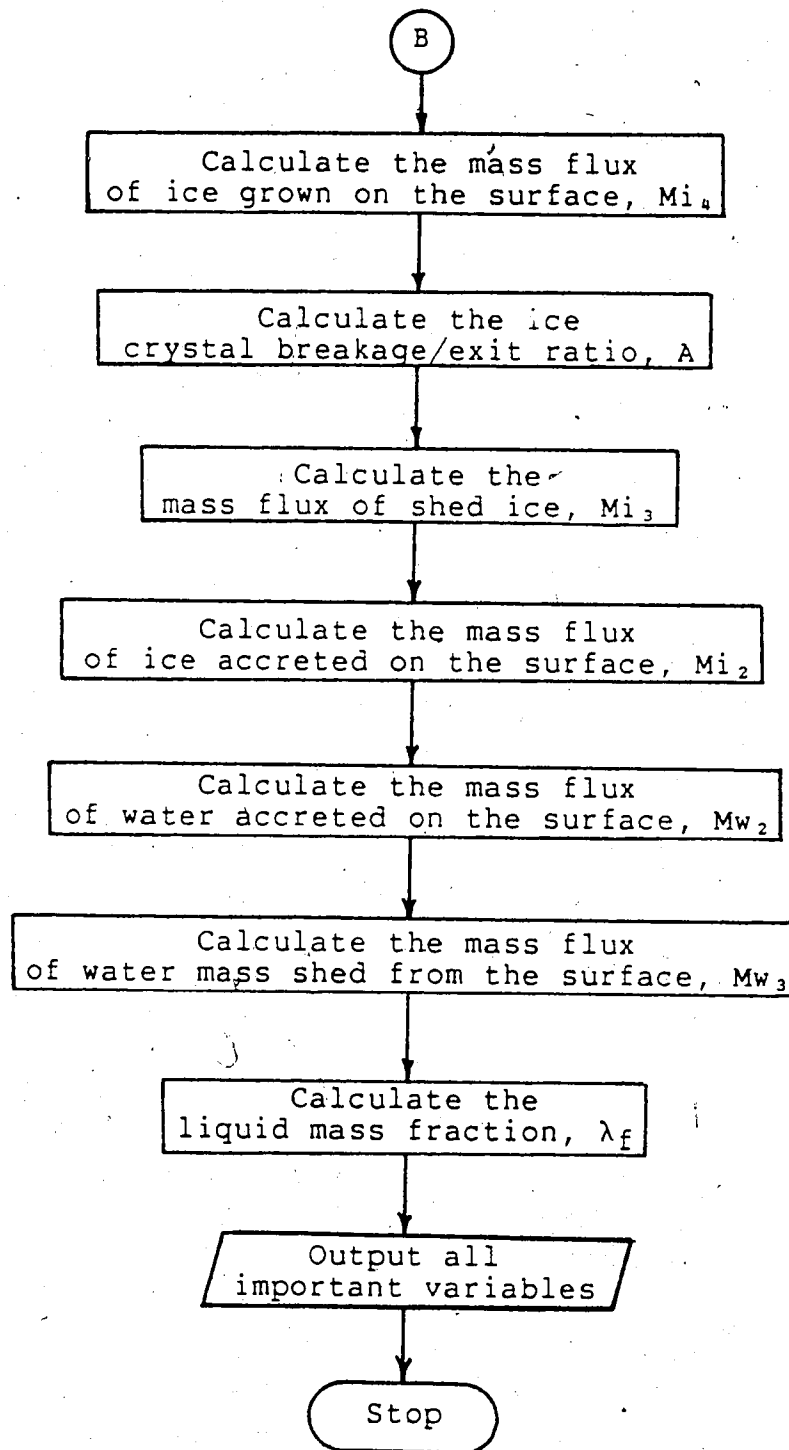
$Mi_a$  represents a maximum potential growth flux of ice to the growing surface. If the flux of collected liquid  $Mw_i$  is smaller than  $Mi_a$ , the icing is assumed to be dry and consequently not a spongy formation. Under these circumstances, the availability of liquid water would control the mass accretion rate. Equation B.7 is thus used to model the mass growth of pure ice at the surface of the spongy accretion.

## Appendix C

The program described here is designed to calculate the liquid water content for a freshwater spongy spray icing model (on a rotating cylinder). The model equations are given in section 5.3. First a flow chart is presented, then a Fortran program is listed and finally an output example.







A list of variables follows in the order that they first appear in the following program. The program variable is given first, followed by the variable name (in brackets) as given in the main text. This is followed by a brief description of the variable.

MPI1 ( $M_{i1}$ ) - the mass flux of pure ice particles collected  
 MPW1 ( $M_{w1}$ ) - the mass flux of pure water collected  
 MPI2 ( $M_{i2}$ ) - the mass flux of ice accreted  
 MPW2 ( $M_{w2}$ ) - the mass flux of pure water  
 MPI3 ( $M_{i3}$ ) - the mass flux of shed ice particles  
 MPW3 ( $M_{w3}$ ) - the mass flux of shed pure water  
 MPIT ( $M_{i4}$ ) - the maximum potential accretion flux of ice  
 LV ( $L_e$ ) - the latent heat of evaporation  
 LF ( $L$ ) - the latent heat of fusion  
 NU ( $Nu$ ) - the Nusselt number for the cylinder  
 MU ( $\mu$ ) - the dynamic viscosity of air  
 KA ( $k_a$ ) - the thermal conductivity of air  
 L, LWC ( $w$ ) - the liquid water content  
 K, KO - the inertial parameter and the modified inertial parameter (for collection efficiency calculation)  
 D0, D1, D2, D3, D4 - empirical constant for the saturation vapor pressure of air  
 TS ( $t_s$ ) - the temperature of the icing surface  
 PR ( $Pr$ ) - the Prandtl number  
 SC ( $Sc$ ) - the Schmidt number  
 PRES ( $P_a$ ) - air pressure  
 CP ( $c_p$ ) - the specific heat of air at constant pressure  
 CW ( $c_w$ ) - the specific heat of water  
 CI ( $c_i$ ) - the specific heat of ice  
 EPS ( $\epsilon$ ) - the ratio of the molecular weight of water to that of air  
 RD ( $R_d$ ) - the gas constant for dry air  
 SIGMA ( $\sigma$ ) - the Stefan-Boltzmann constant  
 AS ( $a$ ) - the linearized radiation constant  
 RHOW - the density of water  
 RHOI - the density of pure ice  
 PI ( $\pi$ ) -  $\pi$ , the constant  
 VWIND ( $V_a$ ) - the air speed  
 TAIR ( $t_a$ ) - the air temperature  
 TDROP ( $t_d$ ) - the droplet temperature  
 DCYL ( $D$ ) - the accretion diameter  
 OMEGA ( $\Omega$ ) - the rate of rotation (radians/second)  
 DDROP ( $d$ ) - the median volume diameter of the droplets  
 RO - the density of gas  
 RED - droplet Reynolds number  
 EM - collection efficiency for a monodisperse droplet size  
 E ( $E$ ) - collection efficiency for a median volume droplet size  
 RE ( $Re$ ) - Reynolds number for the cylinder

H (h) - overall heat transfer coefficient for a cylinder  
 PART1,PART2,PART3 - heat transfer factors for the MPIT  
 equation  
 EAIR,ETS ( $e_a, e_s$ ) - the saturation water vapour pressures  
 over water at the dew point and surface temperature,  
 respectively  
 FRALIQ ( $\lambda_f$ ) - the freshwater liquid mass fraction  
 FN ( $n_f$ ) - the freezing fraction  
 R1,R2,R3 - the total collected, accreted and shed fluxes,  
 respectively.

C  
 C  
 C

A FRESH WATER SPONGY ICING MODEL

REAL MPI1,MPW1,MPI2,MPW2,MPI3,MPW3,MPIT,  
 &LV,LF,NU,MU,KA,L,LWC,K,KO  
 D0=6.107799961  
 D1=4.436518521E-01  
 D2=1.428945805E-02  
 D3=2.650648471E-04  
 D4=3.031240396E-06

C  
 C  
 C

DEFINE CONSTANTS

MPI1=0.0  
 TS=0.0  
 PR=0.711  
 SC=0.595  
 PRES=1.0E+05  
 LV=2.5E+06  
 LF=3.34E+05  
 CP=1005.0  
 CW=4270.0  
 CI=2070.0  
 EPS=0.6221  
 RD=287.04  
 SIGMA=5.67E-08  
 AS=8.1E+07  
 RHOW=1000.0  
 RHOI=917.0  
 PI=3.1416  
 4 CONTINUE\*

C  
 C  
 C

INPUT PROMPTS

WRITE (6,5)  
 5 FORMAT ( /, 'WIND SPEED (M/S)?')  
 CALL FREAD (5, 'R:', VWIND)  
 WRITE (6,10) VWIND  
 WRITE (7,10) VWIND  
 10 FORMAT ( ' ', 'WIND SPEED=', F6.1)  
 WRITE (6,20)



```

C
C CALCULATE THE HEAT TRANSFER COEFFICIENT
C
RE=VWIND*DCYL*RO/MU
NU=.24*RE**0.6
H=KA*NU/DCYL
C CALCULATE FACTORS FOR THE HEAT BALANCE
PART1=PI*DCYL*H/LF
PART2=(PR/SC)**0.63*EPS*LV/(CP*PRES)
PART3=PI*DCYL*SIGMA*AS
EAIR=D0+TAIR*(D1+TAIR*(D2+TAIR*(D3+TAIR*D4)))
EAIR=EAIR*100.0
ETS=D0+TS*(D1+TS*(D2+TS*(D3+TS*D4)))
ETS=ETS*100.0
C CALCULATE THE ICE ACCRETION MASS FLUX
MPIT=PART1*((TS-TAIR)+PART2*(ETS-EAIR))
MPIT=MPIT+(1.0/LF)*(MPI1*CI+MPW1*CW)*(TS-TAIR)
MPIT=MPIT+(1.0/LF)*PART3*(TS-TAIR)
C DRY ICING DECISION
IF(MPIT.GE.MPW1) GO TO 800
C OUTPUT COLLECTION AND THERMODYNAMIC COEFFICIENTS
WRITE(6,220)RO,MU,KA,RE,NU,H,
&PART1,PART2,PART3,EAIR,ETS,MPIT
WRITE(7,220)RO,MU,KA,RE,NU,H,
&PART1,PART2,PART3,EAIR,ETS,MPIT
220 FORMAT(' ', 'RO=', E10.4, ' MU=', E10.4, ' KA=', E10.4, /,
& ' RE=', E10.4, ' NU=', E10.4, ' H=', E10.4, /,
& ' PART1=', E10.4, ' PART2=', E10.4, ' PART3=', E10.4, /,
& ' EAIR=', E10.4, ' ETS=', E10.4, ' MPIT=', E10.4, /)
C CALCULATE THE ICE CRYSTAL BREAKAGE/EXIT RATIO
A=17.514*(MPIT/(MPW1-MPIT))**0.9879*
&((MPW1-MPIT)/MPW1)**3.800*
&(OMEGA*DCYL/VWIND)**0.6602*
&(9.81/(OMEGA**2*DCYL))**0.5778
C CALCULATE THE SHED ICE MASS FLUX
MPI3=A*MPIT+MPI1
C CALCULATE THE ICE ACCRETION MASS FLUX
MPI2=MPI1+MPIT-MPI3
C CALCULATE THE WATER ACCRETION MASS FLUX
MPW2=(RHOW/RHOI)*(MPIT-MPI2)
C CALCULATE THE SHED WATER MASS FLUX
MPW3=(MPI1+MPW1)-(MPI2+MPW2)-MPI3
C CALCULATE THE LIQUID FRACTION OF THE ACCRETION
FRALIF=100.0*MPW2/(MPI2+MPW2)
R1=MPI1+MPW1
R2=MPI2+MPW2
R3=MPI3+MPW3
FN=MPIT/MPW1
WRITE(6,720)A,FRALIF,MPIT,FN,MPI1,MPW1,
&R1,MPI2,MPW2,R2,MPI3,MPW3,R3
WRITE(7,720)A,FRALIF,MPIT,FN,MPI1,MPW1,
&R1,MPI2,MPW2,R2,MPI3,MPW3,R3
720 FORMAT(' A=', E10.4, ' L.F.=', F7.3, '% MPIT=', E10.4,
& ' n=', F7.4, /,

```

```

&' MPI 1=' ,E10.4, ' MPW1=' ,E10.4, ' R1=' ,E10.4, //,
&' MPI 2=' ,E10.4, ' MPW2=' ,E10.4, ' R2=' ,E10.4, //,
&' MPI 3=' ,E10.4, ' MPW3=' ,E10.4, ' R3=' ,E10.4, //)
GO TO 820
800 CONTINUE
WRITE(6,810)
WRITE(7,810)
810 FORMAT(' ', ' DRY ICING: MPIT>MPW1' ,//)
820 CONTINUE
WRITE(6,830)
830 FORMAT(' ', 'ENTER 1.0 TO RERUN')
CALL FREAD(5, 'R:', DECIS)
IF(DECIS.EQ.1.0) GO TO 4
STOP
END

```

#### An Example of Output

```

WIND SPEED= 23.0
AIR TEMP= -3.0 DROP TEMP= -3.0
LIQUID WATER CONTENT= 0.0017KG/CUBIC METER
CYLINDER DIAMETER= 0.0500 OMEGA= 0.500
DROP DIAMETER= 0.1600E-04
K= 0.7685E+00 RED= 0.2787E+02 K0= 0.4092E+00 EM= 0.1729E+00
E= 0.2295E+00

RO=0.1290E+01 MU=0.1703E-04 KA=0.2408E-01
RE=0.8710E+05 NU=0.2209E+03 H=0.1064E+03
PART1=0.5004E-04 PART2=0.1731E-01 PART3=0.7214E+00
EAIR=0.4899E+03 ETS=0.6108E+03 MPIT=0.2785E-03

A=0.1496E+00 L.F.= 16.092% MPIT=0.2785E-03 n= 0.6209
MPI 1=0.0 MPW1=0.4486E-03 R1=0.4486E-03
MPI 2=0.2369E-03 MPW2=0.4543E-04 R2=0.2823E-03
MPI 3=0.4166E-04 MPW3=0.1246E-03 R3=0.1663E-03

```

## Appendix D

The experimental method described in section 5.4 did not allow for direct measurement of the droplet diameter. The method used to infer a median volumetric drop diameter is presented here along with the resulting droplet sizes for the data shown in Fig. 5.1, Fig. 5.2, and Fig. 5.3. The median volumetric diameter for the data in Fig. 5.4 could not be estimated in the same manner, so it was assumed to be 25  $\mu\text{m}$ , the same as in Fig. 5.3. This represents an arbitrary, but perhaps not unreasonable choice, since the same spray nozzle was used in each case.

The reason that the data in Fig. 5.4 could not be used in the same way as that from Figures 5.1, 5.2 and 5.3, is that there was no data close to the Ludlam limit (wet/dry icing transition point). Figures 5.1, 5.2 and 5.3 show the variation of sponginess as a function of air temperature and consequently in each case, the transition from wet icing to dry icing is shown. It is at the Ludlam limit that all of the collected water mass flux  $M_w = M_i$ , the maximum potential ice growth flux.

The Ludlam limit offers a convenient thermodynamic condition for determining the median volumetric diameter,  $d$ . It is assumed that there is no liquid shed from the surface (ie: all collected water is solidified on the surface), and that the surface temperature is 0 °C for freshwater icing. Because there is no liquid shedding, the collected water mass flux may be modelled assuming no bouncing or splashing

that may be present with shedding water films. Also, the heat transfer can be determined on the basis of an assumed 0 °C surface temperature with less concern for the possibility of incomplete surface water film mixing before shedding inherent in wet icing.

The present approach assumes heat transfer from a non-rotating smooth cylinder (Zukauskas, 1972), and collection mechanics based on the Langmuir and Blodgett (1949) data. The median volume drop diameter equation for overall collection efficiency of Bain and Gayet (1982) is used, along with the improved correlation for the overall median volume diameter droplet collection efficiency of Cansdale and McNaughton (1977).

The method assumes that there is a unique droplet size which will yield a collection efficiency such that the collected water mass flux will be completely solidified and stay on the cylinder. At the Ludlam limit, the cylinder cooling must just equal the latent heat released on the surface of the cylinder by solidifying water. The surface cooling depends on the temperature of the icing surface (assumed to be 0 °C) and the temperature of the surroundings (the air, droplets and surroundings are assumed to have the same temperature). For a given set of environmental conditions, the temperature of the surroundings at which all the collected water is just solidified, is here called the Ludlam limit temperature. The Ludlam limit temperature is assumed to be the temperature at which an accretion contains



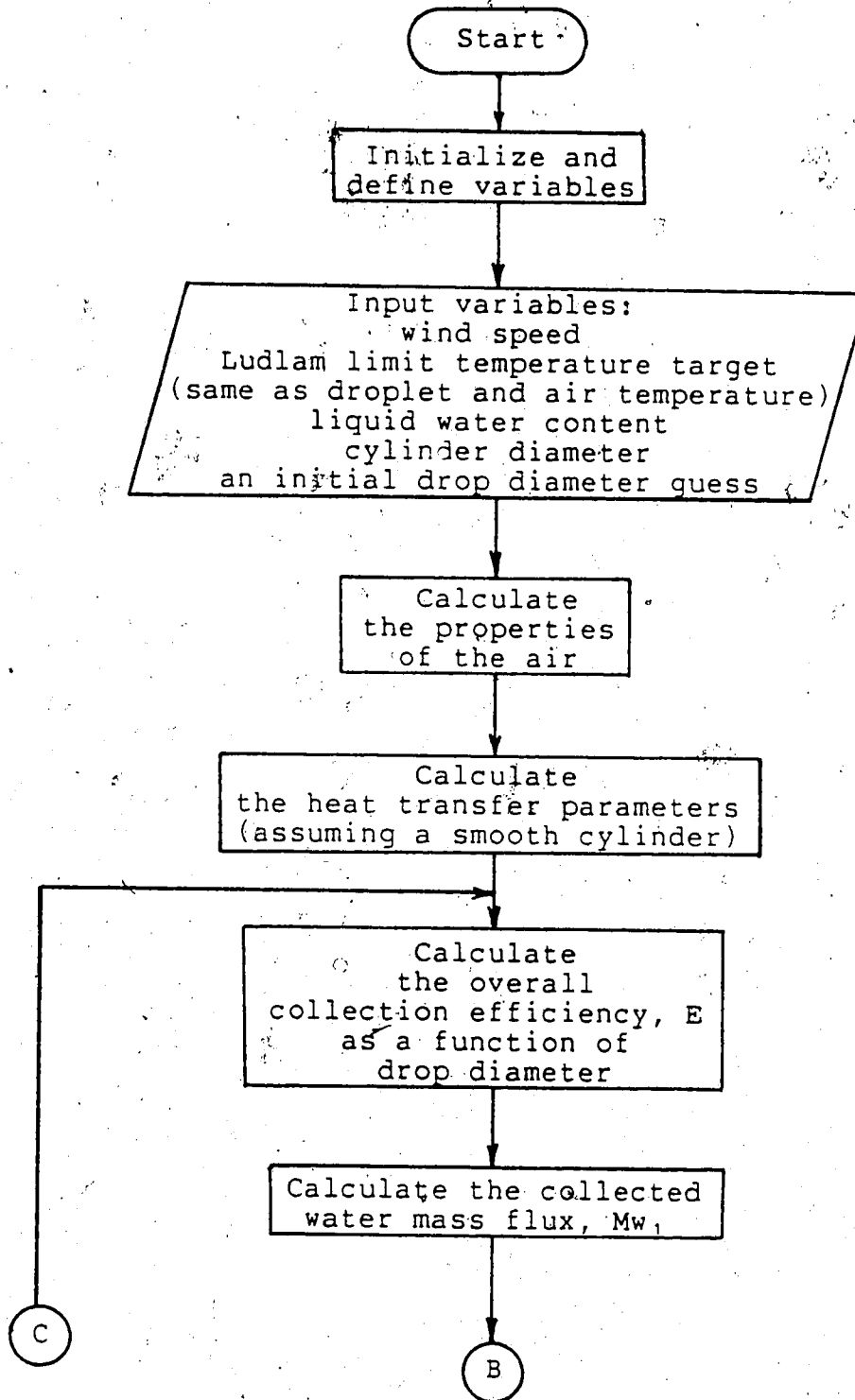
no liquid water ( $\lambda_f=0$ ; not spongy), and the surface is still assumed (in freshwater spray icing), to be at the equilibrium freezing temperature, with no liquid film. Using these criterion, the Ludlam limit temperature for figures 5.1, 5.2 and 5.3 were chosen as  $-4.6$  °C,  $-8.0$  °C, and  $-13.5$  °C. The environmental temperature at which the surface liquid film, inherent in wet icing, and the inclusion of liquid water, inherent in spongy icing, are no longer apparent is the temperature required to find the median volume droplet diameter.

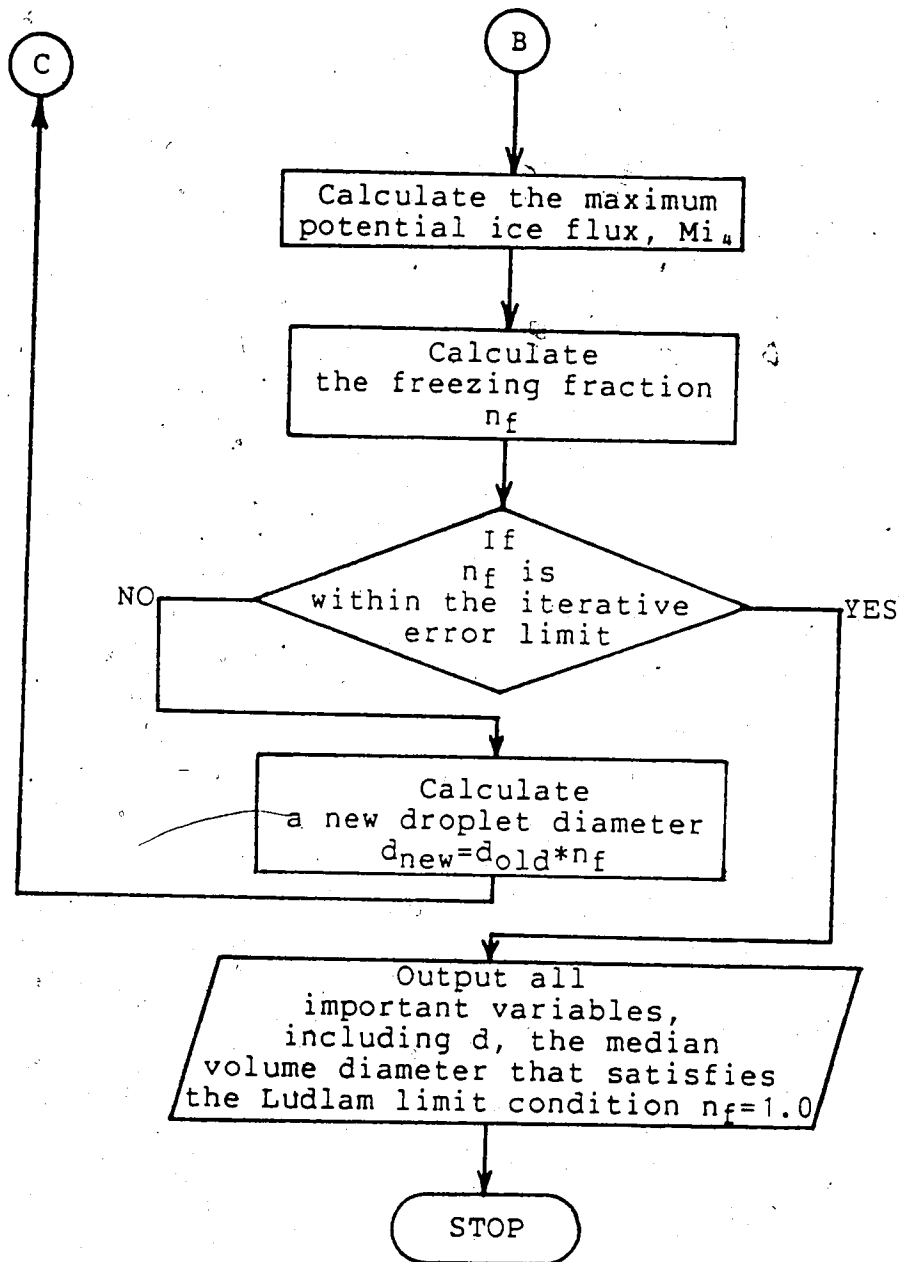
The median volume diameter is solved with the algorithm shown in the following flow chart. Initially, the environmental conditions are input along with the Ludlam limit temperature and a first guess at  $d$ , the median volume diameter. The properties of the air, and the heat transfer parameters are calculated on the basis of the environmental conditions. Next, the first iterative value of the drop diameter is used to calculate the collection efficiency,  $E$ . Once  $E$  is known, both the collected water,  $M_w$ , and the solidification flux  $M_i$ , are calculated. The solid growth freezing fraction is calculated as a result. If it is sufficiently close to one, the initial drop diameter guess is accepted. However, much more likely is that  $n_f$  will not be sufficiently close to 1.0 and a new value of drop diameter is subsequently assigned. The new value of drop diameter is assigned as a result of multiplying the old value by the freezing fraction,  $n_f$ , ( $d_{new} = d_{old}n_f$ ). This new

value of drop diameter is used to calculate a new collection efficiency, collection flux, solidification flux, and  $n_f$ . The iteration is terminated when  $n_f$  is sufficiently close to unity, and then the acceptable median volume diameter is output.

This method was found to converge in all the cases that had a Ludlam limit. However, the reader is warned that if the environmental conditions are specified in such a way that only dry icing is possible, then the search for a median volume droplet diameter will result in an unstable numerical solution.

This method of determining median volume drop diameter depends on the following assumptions: (1) availability of sufficient data around the Ludlam limit condition; (2) an accurate collection mechanics assumption; (3) accurately modelled heat transfer, and (4) that the spray system delivers droplet size independent of variations in the tunnel conditions, such as air temperature or air speed.





Most of the variables in the following program are listed in the parameter list of Appendix C. Those that are in this program, but not in the above list, are noted below.

NF,NFNEW ( $n_f$ ) - variables that contain iterative values of the freezing fraction  
 KOUNT - parameter used to report the number of iterations used before the error tolerance is satisfied  
 TDROP,TAIR - the Ludlam limit temperature is equal to both the droplet temperature and the air temperature (thermal equilibrium is assumed between the air and water droplets)

```

C
C   A PROGRAM TO FIND THE DROPLET DIAMETER
C   FOR A SPECIFIED LUDLAM LIMIT TEMPERATURE
C
      REAL MPW1,MPIT,NF,NFNEW,LV,LF,NU,MU,KA,L,LWC,K,KO
      D0=6.107799961
      D1=4.436518521E-01
      D2=1.428945805E-02
      D3=2.650648471E-04
      D4=3.031240396E-06
C   DEFINE CONSTANTS
      NF=1.0
      TS=0.0
      PR=0.711
      SC=0.595
      PRES=1.0E+05
      LV=2.5E+06
      LF=3.34E+05
      CP=1005.0
      CW=4270.0
      CI=2070.0
      EPS=0.6221
      RD=287.04
      SIGMA=5.67E-08
      AS=8.1E+07
      RHOW=1000.0
      RHOI=917.0
      PI=3.1416
      KOUNT=0
      INPUT PROMPTS
      WRITE (6,5)
5  FORMAT ( /, 'WIND SPEED (M/S)?' )
      CALL FREAD (5, 'R:', VWIND)
      WRITE (6,10) VWIND
      WRITE (7,10) VWIND
10  FORMAT ( ' ', 'WIND SPEED=', F6.1, ' m/s' )
      WRITE (6,20)
20  FORMAT ( /, 'ENTER THE LUDLAM LIMIT TEMPERATURE (deg
C)', /,
      &' (ASSUMED EQUAL TO BOTH THE AIR AND DROP
TEMPERATURES)' )
      CALL FREAD (5, '2R:', TAIR, TDROP)
      WRITE (6,30) TAIR, TDROP
      WRITE (7,30) TAIR, TDROP
30  FORMAT ( ' ', 'AIR TEMP=', F6.1, ' deg C',

```

```

&' DROP TEMP=',F6.1,' deg C')
WRITE (6,40)
40 FORMAT ( /, 'LIQUID WATER CONTENT-GMS/CUBIC METER?')
CALL FREAD (5, 'R:', L)
LWC=L/1000.0
WRITE (6,50) LWC
WRITE (7,50) LWC
50 FORMAT ( ' ', 'LIQUID WATER CONTENT=',F11.4,' Kg/m^3')
WRITE (6,60)
60 FORMAT ( /, 'CYL.DIA. METERS')
CALL FREAD (5, 'R:', DCYL)
WRITE (6,70) DCYL
WRITE (7,70) DCYL
70 FORMAT ( ' ', 'CYLINDER DIAMETER=',F9.4,' m')
WRITE (6,80)
80 FORMAT ( /, 'INITIAL DROP DIAMETER GUESS-MICROMETERS?')
CALL FREAD (5, 'R:', DDROP)
DDROP=DDROP/1.0E+06
WRITE (6,90) DDROP
WRITE (7,90) DDROP
90 FORMAT ( ' ', 'DROP DIAMETER=',E11.4,' m')
C CALCULATE FUNCTIONS OF AIR TEMPERATURE:
C AIR DENSITY, DYNAMIC VISCOSITY, CONDUCTIVITY
RO=PRES/(RD*(TAIR+273.16))
MU=1.718E-05+5.1E-08*TAIR
KA=.0243+.000073*TAIR
C CALCULATE THE HEAT TRANSFER COEFFICIENT
RE=VWIND*DCYL*RO/MU
NU=.24*RE**0.6
H=KA*NU/DCYL
C CALCULATE FACTORS FOR THE HEAT BALANCE
PART1=PI*DCYL*H/LF
PART2=(PR/SC)**0.63*EPS*LV/(CP*PRES)
PART3=PI*DCYL*SIGMA*AS
EAIR=D0+TAIR*(D1+TAIR*(D2+TAIR*(D3+TAIR*D4)))
EAIR=EAIR*100.0
ETS=D0+TS*(D1+TS*(D2+TS*(D3+TS*D4)))
ETS=ETS*100.0
C OUTPUT COLLECTION AND THERMODYNAMIC COEFFICIENTS
WRITE(6,95)RO,MU,KA,RE,NU,H,PART1,PART2,PART3,EAIR,ETS
WRITE(7,95)RO,MU,KA,RE,NU,H,PART1,PART2,PART3,EAIR,ETS
95 FORMAT(' ', 'RO=',E10.4,' MU=',E10.4,' KA=',E10.4,/,
&' RE=',E10.4,' NU=',E10.4,' H=',E10.4,/,
&' PART1=',E10.4,' PART2=',E10.4,' PART3=',E10.4,/,
&' EAIR=',E10.4,' ETS ',E10.4,/)
C CALCULATE THE OVERALL COLLECTION EFFICIENCY
100 CONTINUE
K=RHOW*VWIND*DDROP**2/(9.0*MU*DCYL)
RED=VWIND*DDROP*RO/MU
K0=K/(0.087*RED**(0.76*RED**(-1.0*0.027))+1.0)
EM=0.0
IF (K0.GT.0.125) EM=0.5*(ALOG10(8.0*K0))**1.6
IF (K0.GT.0.8) EM=K0**1.1/((K0**1.1)+1.426)
E=.69*EM**.67+.31*EM**1.67

```

```

C      WRITE(6,150) K,RED,K0,EM,E
C      WRITE(7,150) K,RED,K0,EM,E
C 150  FORMAT(' ', 'K=',E11.4, ' RED=',E11.4, ' K0=',E11.4,
C      &' EM=',E11.4, ' E=',E11.4)
C      CALCULATE THE COLLECTED LIQUID MASS FLUX
C      MPW1=E*VWIND*LWC*DCYL
C      CALCULATE THE ICE ACCRETION MASS FLUX
C      MPIT=PART1*((TS-TAIR)+PART2*(ETS-EAIR))
C      MPIT=MPIT+(1.0/LF)*(MPW1*CW)*(TS-TAIR)
C      MPIT=MPIT+(1.0/LF)*PART3*(TS-TAIR)
C      CALCULATE FREEZING FRACTION NF
C      NFNEW=MPIT/MPW1
C      OUTPUT
C      WRITE(6,210)MPIT,MPW1,NFNEW,DDROP,E
C 210  FORMAT(' ', ' MPIT=',E10.4, ' MPW1=',E10.4,
C      &' NFNEW=',E10.4,/, ' DROP DIA=',E10.4, ' E=',E10.4)
C      ITERATIVE DECISION
C      IF(ABS(1.0-NFNEW/NF).LT.0.0001) GO TO 500
C      KOUNT=KOUNT+1
C      DDROP=DDROP*NFNEW
C      NF=NFNEW
C      GO TO 100
500  CONTINUE
C      FINAL OUTPUT
C      WRITE(7,550)MPIT,MPW1,NF,NFNEW,E,DDROP,TAIR,KOUNT
550  FORMAT(' ', 'MPIT=',E10.4, ' MPW1=',E10.4,
C      &' BOTH IN (Kg/ms)',/,
C      &' NF=',E10.4, ' NFNEW=',E10.4, ' E=',E10.4,/,
C      &' THE LUDLAM LIMIT DROP DIAMETER=',E10.4, ' m',/,
C      &' FOR A LUDLAM LIMIT TEMPERATURE=',F7.2, ' deg C',/,
C      &' ITERATIONS REQUIRED ',I4)
C      STOP
C      END

```

The following trials were run to establish the characteristic droplet diameter for each of the first three data sets. Upon the basis of these runs the median volumetric diameters were selected for Figures 5.1 to 5.3.

TRIAL 1 (FIGURE 5.1)

WIND SPEED= 23.0 m/s  
 AIR TEMP= -4.7 deg C DROP TEMP= -4.7 deg C  
 LIQUID WATER CONTENT= 0.0017 Kg/m<sup>3</sup>  
 CYLINDER DIAMETER= 0.0500 m  
 DROP DIAMETER= 0.2000E-04 m  
 RO=0.1298E+01 MU=0.1694E-04 KA=0.3396E-01  
 RE=0.8810E+05 NU=0.2224E+03 H=0.1066E+03  
 PART1=0.5012E-04 PART2=0.1731E-01 PART3=0.7214E+00  
 EAIR=0.4312E+03 ETS=0.6108E+03

MPIT=0.4272E-03 MPW1=0.4272E-03 BOTH IN (Kg/ms)  
 NF=0.1000E+01 NFNEW=0.1000E+01 E=0.2185E+00  
 THE LUDLAM LIMIT DROP DIAMETER=0.1554E-04 m  
 FOR A LUDLAM LIMIT TEMPERATURE= -4.70 deg C  
 ITERATIONS REQUIRED 22

TRIAL 2 (FIGURE 5.2)

WIND SPEED= 28.0 m/s  
 AIR TEMP= -8.0 deg C DROP TEMP= -8.0 deg C  
 LIQUID WATER CONTENT= 0.0017 Kg/m<sup>3</sup>  
 CYLINDER DIAMETER= 0.0500 m  
 DROP DIAMETER= 0.2500E-04 m  
 RO=0.1314E+01 MU=0.1677E-04 KA=0.2372E-01  
 RE=0.1097E+06 NU=0.2537E+03 H=0.1203E+03  
 PART1=0.5659E-04 PART2=0.1731E-01 PART3=0.7214E+00  
 EAIR=0.3350E+03 ETS=0.6108E+03

MPIT=0.8245E-03 MPW1=0.8245E-03 BOTH IN (Kg/ms)  
 NF=0.1000E+01 NFNEW=0.1000E+01 E=0.3464E+00  
 THE LUDLAM LIMIT DROP DIAMETER=0.1953E-04 m  
 FOR A LUDLAM LIMIT TEMPERATURE= -8.00 deg C  
 ITERATIONS REQUIRED 5

TRIAL 3 (FIGURE 5.3)

WIND SPEED= 20.0 m/s  
 AIR TEMP= -13.5 deg C DROP TEMP= -13.5 deg C  
 LIQUID WATER CONTENT= 0.0030 Kg/m<sup>3</sup>  
 CYLINDER DIAMETER= 0.0500 m  
 DROP DIAMETER= 0.2000E-04 m  
 RO=0.1342E+01 MU=0.1649E-04 KA=0.2331E-01  
 RE=0.8136E+05 NU=0.2121E+03 H=0.9888E+02  
 PART1=0.4650E-04 PART2=0.1731E-01 PART3=0.7214E+00



EAIR=0.2171E+03 ETS=0.6108E+03

MPIT=0.1177E-02 MPW1=0.1177E-02 BOTH IN (Kg/ms)  
NF=0.1000E+01 NFNEW=0.1000E+01 E=0.3923E+00  
THE LUDLAM LIMIT DROP DIAMETER=0.2469E-04 m  
FOR A LUDLAM LIMIT TEMPERATURE= -13.50 deg C  
ITERATIONS REQUIRED 4

## Appendix E

The experimental data which were presented in the graphs in Chapter 5 are documented here. Trial 1 through Trial 4 correspond to Figure 5.1 through Figure 5.4, respectively. All of these trials were carried out during the summer of 1986 in the F.R.O.S.T. facility at the University of Alberta.

### TRIAL ONE

Wind speed: 23 m/s

Liquid water content: 1.7 gm<sup>-3</sup>

Cylinder diameter: 5 cm

Rate of rotation: 0.5 Hz

Drop Diameter: 16  $\mu$ m

Air Temperature ( $^{\circ}$ C)	Ice Fraction
-14.0	100.0
-10.0	100.0
-8.2	100.0
-7.0	100.0
-5.8	100.0
-4.8	98.0
-3.4	82.0
-3.2	83.0
-2.2	78.0
-4.2	99.0
-3.6	98.0
-2.5	77.0
-2.0	69.0
-4.6	100.0
-3.0	89.0
-2.7	84.0
-4.1	98.0
-3.0	86.0
-2.7	81.0
-3.5	88.0
-3.6	80.0
-3.7	89.0
-5.9	99.0
-5.4	99.0
-4.9	96.0
-4.5	98.0
-4.1	100.0
-3.7	91.0
-3.5	87.0
-2.0	67.0

## TRIAL TWO

Wind speed: 28 m/s  
 Liquid water content: 1.7 gm<sub>3</sub>  
 Cylinder diameter: 5 cm  
 Rate of rotation: 0.5 Hz  
 Drop diameter: 20 μm

Air Temperature (°C)	Ice Fraction
-14.0	100.0
-13.2	100.0
-11.8	100.0
-10.2	100.0
-9.0	100.0
-8.0	99.0
-6.8	99.0
-4.6	93.0
-3.6	68.0
-2.6	72.0
-4.0	78.0

## TRIAL THREE

Wind speed: 20 m/s  
 Liquid water content: 3.0 gm<sub>3</sub>  
 Cylinder diameter: 5 cm  
 Rate of rotation: 0.5 Hz  
 Drop diameter: 25 μm

Air Temperature (°C)	Ice Fraction
-5.9	66.0
-5.1	64.0
-3.6	60.0
-9.0	80.0
-8.2	79.0
-8.2	84.0
-6.5	79.0
-13.7	100.0
-11.8	100.0
-10.3	88.0
-2.1	57.0

## TRIAL FOUR

Air temperature:  $-5.0^{\circ}\text{C}$   
Liquid water content:  $4.4 \text{ gm}^{-3}$   
Cylinder diameter: 5 cm  
Rate of rotation: 0.5 Hz  
Drop diameter:  $25 \mu\text{m}$

Air Velocity (m/s)

41.6  
38.1  
33.9  
30.4  
27.7  
25.6  
22.1  
19.3  
15.3  
8.4

Ice Fraction

74.0  
73.0  
69.0  
67.0  
57.0  
53.0  
50.0  
48.0  
44.0  
48.0